ADVANCED INTELLIGENT SYSTEMS
Open Access
www.advintellsyst.com

Soft Wearable Rehabilitation Robots with Artificial Muscles based on Smart Materials: A Review

Alberto Gonzalez-Vazquez, Lorenzo Garcia, Jeff Kilby, and Peter McNair*

Wearables robots have gained attention for the rehabilitation of people with physical disabilities. However, the current technology relies on heavy and bulky actuation components, making it hard to use outside clinical settings. Artificial muscles based on smart materials are trending for soft wearable rehabilitation robots as they present advantages of compliance, are lightweight, and do not require external components. Nevertheless, they present challenges that remain unresolved, preventing widespread adoption. This work reviews the current state of soft wearable rehabilitation robots with artificial muscles based on smart materials (AMSMs). A literature search is conducted utilizing Web of Science and Scopus. Based on the inclusion–exclusion criteria, 15 devices are found using four different smart materials. This study attempts to provide an insight into the distinct biomechanical requirements, the use of smart materials, their limitations, their designs, and possible future research directions, which can provide helpful guidance on the implementation and development of advanced soft wearable rehabilitation robots with AMSMs.

1. Introduction

During the past decade, wearable devices such as exoskeletons have gained popularity[1] in different fields, such as the military,[2] industry,[3] and rehabilitation.[4] In the latter, rehabilitation exoskeletons are used to restore or maintain the functionality and mobility of people with physical disabilities.[5] These are receiving greater attention as the number of people with disabilities affecting physical performance will increase in the following decades as the population ages and individuals live longer with noncommunicable conditions (e.g., cerebral palsy, stroke, acquired brain injuries, and muscular dystrophies).[6–8]

Most current exoskeletons use electric motors and rigid links to realize actuation and often have heavy and bulky designs that are difficult to safely wear outside clinical facilities.[9] Hence, researchers in this area are working to develop soft wearable rehabilitation robots (SWRRs), featuring soft actuators that are agreeable to the users as they have increased compliance, adaptability, comfort, safety, and less weight.[10–12]

Currently, SWRR relies mainly upon two soft robotic technologies, cable-driven and fluidic actuators. For a cable-driven system, the wire is embedded into clothes or tubes and attached to an anchor point. The other side of the wire is connected to an electric motor to generate the desired movement and force by pulling the cable[13,14] (**Figure 1**a). Alternatively, in fluidic actuation (Hydraulic/Pneumatic), a pressurized fluid is inserted into a chamber made of highly deformable material to generate a displacement[11,15,16] (Figure 1b). However, these require large and heavy external pumps and valves to compress the fluid.[17] Unfortunately, cable-driven and fluidic actuation need cumbersome components (e.g., electric motors, pumps, and valves) to work, compromising the portability of the systems when used in daily life.[18]

Therefore, in recent years, research has been committed to developing new actuator technologies that can overcome the drawbacks of the current actuators used in SWRR. These technologies include artificial muscles based on smart materials (AMSMs). AMSMs are soft actuators composed primarily of material with a low Young's modulus similar to that of soft biological materials (10^4–10^9 Pa) that can sense and directly convert physical stimulus (e.g., light, electrical, heat) into physical displacement.[19–23] Some examples of smart materials are shape-memory alloy (SMA),[24] dielectric elastomer actuators (DEAs),[25] ionic polymer–metal composites (IPMC),[26] shape-memory polymers (SMPs),[27] and twisted and coiled polymer actuators (TCPs).[28] Due to their inherent properties and manufacturing processes, AMSM can be fabricated in various shapes, allowing them to be embedded into flexible and deformable wearable devices.[29–32] Furthermore, it is possible to fabricate robots with a relatively small weight and volume as they present a power density comparable to the skeletal muscles.[33]

Nevertheless, AMSMs for rehabilitation robots are still at the early stage of development. Some drawbacks specific to every

A. Gonzalez-Vazquez, L. Garcia, J. Kilby
BioDesign Lab
School of Engineering
Computer and Mathematical Sciences
Auckland University of Technology
Auckland 1010, New Zealand
E-mail: lorenzo.garcia@aut.ac.nz

P. McNair
Health and Rehabilitation Research Institute
Auckland University of Technology
Auckland 1010, New Zealand

The ORCID identification number(s) for the author(s) of this article can be found under https://doi.org/10.1002/aisy.202200159.

DOI: 10.1002/aisy.202200159

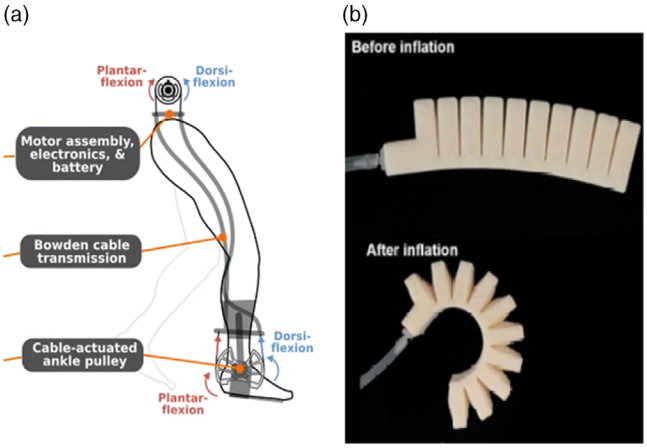

Figure 1. a) Ankle foot orthosis cable-driven system schematic providing plantar-flexion and dorsiflexion assistance. Reproduced with permission.[14] Copyright 2019, Springer Nature. b) Pneumatic actuator before and after inflation. Reproduced with permission.[16] Copyright 2020, IEEE.

smart material (e.g., low speed in SMA and TCPs and low force generation in DEAs and ionic polymer–metal composites) need to be tackled if they are to become widespread technology utilized in SWRR.[33,34]

The purpose of this article was to review soft wearable rehabilitation robots (SWRR) incorporating AMSM; seeks to: a) identify the biomechanical requirements for these robots; b) identify the different AMSM technologies utilized; b) identify the AMSM limitations for these robots; c) describe the AMSM enhancement design techniques; d) discuss future trends for development in the field of SWRR based on AMSM.

2. Findings

Based on the keywords, 2141 publications were found, with 1193 publications from Web of Science, 948 publications from Scopus, and 4 from a search on the university library.

First, a check was made for duplicated publications. Thereafter, the abstracts of 1466 publications were screened, and 186 titles were selected for full-text reading. After carefully applying the exclusion criteria to the fully read articles, 36 publications were selected. Among the chosen publications, 8 were reviews, and 28 discussed the development and characteristics of the device (**Figure 2** shows a flow diagram that illustrates the process of the selection of the articles).

Six of the eight reviews were focused on compliant actuators for rehabilitation systems and partially included AMSM as part of their scope. Peng et al.[20] focused on soft robots for rehabilitation and nursing care, but most of the analysis was centered on soft robots driven by electric motors and pneumatics. Shahid et al.[35] investigated the soft robotic devices designed for hand rehabilitation, where one device based on AMSM was included. Veale et al.[18] analyzed the current technology on compliant actuators, addressing the potential of new smart materials to be used in wearable exoskeletons. Zhu et al.[23] looked at the developments in soft wearable robots, covering the diverse application of AMSM where rehabilitation robots were included. Bardi

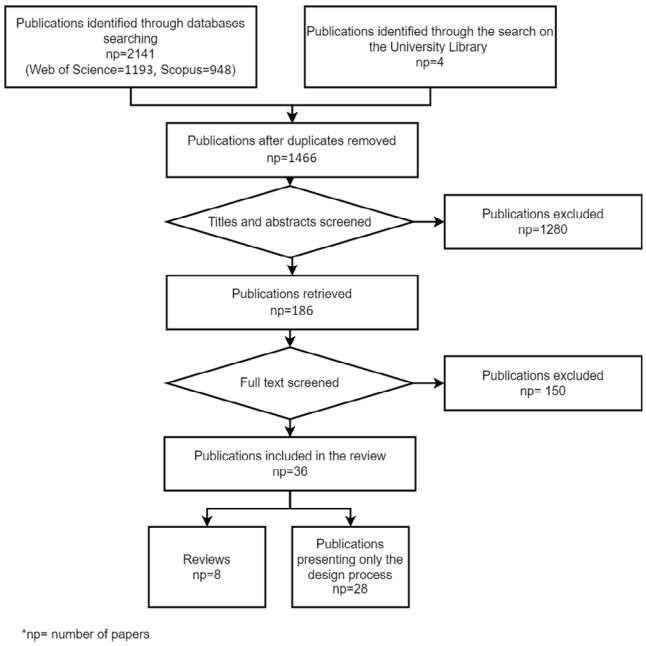

Figure 2. Literature search flow diagram.

et al.[36] researched SWRR for the upper limb, where a section of devices using SMA was included. Finally, Aliseichik et al.[37] went through different artificial muscle technologies, including sections related to SMA and electroactive polymers (EAPs). Two reviews focused on specific smart materials, namely the SMA (Nematollahi et al.[38]) or DEA and plasticized polyvinyl chloride gel (PVC) (Dong et al.[39]) in rehabilitation robots. The difference between the previous review articles and this work is that the earlier articles only partially covered the SWRR based on AMSM, as their scope was more related to soft actuators in general without a focused analysis of AMSM.

Within the 28 focused articles, 4 different types of AMSM technologies were found. Moreover, 17 SWRRs were noticed, 11 systems were designed for the upper limb, especially for treating the wrist and fingers, 5 for the lower limb, and 1 for the face.

3. Discussion

This section is divided into five parts. The first part (3.1) discusses the different biomechanical requirements used in the design of the SWRR. The second part (3.2) presents the different AMSMs and the SWRR that use each technology. The next part (3.3) focuses on the challenges that the SWRR faces. Followed by a part that (3.4) is concerned with how the robot's design can enhance the AMSM properties. Finally in (3.5), future developments are discussed.

3.1. Biomechanical Considerations

During the past decade, wearable exoskeletons have gained popularity[1] in different fields like military, industrial, and

rehabilitation.[3] Each of these fields has different applications and purposes, sometimes with partial overlap. Military exoskeletons are intended to enhance the physical capabilities and increase the mobility of soldiers during load carriage.[40] Industrial exoskeletons focus on augmentation and reinforcing a worker's performance to increase productivity and lower the risk of injury.[3] In contrast, the rehabilitation exoskeleton's purpose is to restore the functionality and mobility of people with a physical disability and whose functional performance is often severely affected.[5]

Moreover, another difference between military and industrial robots compared to rehabilitation robots is the range of populations they cover. For instance, military and industrial systems are mainly focused on healthy adults as beneficiaries. Concerning rehabilitation robots, there is a vast spectrum within the target population requiring different amounts of assistance, from children to the elderly,[41,42] different levels of disabilities,[43] and different types of diseases.[44]

This variability in the target population has led to a different specification for each group as SWRR based on AMSM are in a developmental stage and still present limitations compared to traditional robots.[18,20] Because of this, it is essential to appreciate the biomechanical requirements to develop a helpful SWRR. Furthermore, it will be valuable to understand the advantages and limitations of each AMSM.

Different biomechanical parameters can severely restrict the range of SWRRs that could be utilized in rehabilitation. These parameters are the degree of freedom (DOF) (number of planes of motion, e.g., flexion, extension supination, pronation at the elbow joint), range of motion (ROM), frequency (the maximum frequency that the actuator can be excited continuously), angular velocity (maximum during functional activity), the torque produced, device/system weight, and control scheme.[45] These parameters change depending on the joint, as each of them moves limbs with different mass and lengths, often with different moments of inertia, and is used to perform different activities. In **Table 1–8**, the biomechanical parameters of the biological joints and the SWRRs are presented to allow easy comparison between them.

3.1.1. DOF

In respect of planes of motion, most robot DOFs vary from one to three, depending on the joint. Only three devices have covered all the DOFs observed in human joints. Of note, more DOFs are apparent in robots for the upper limb. This could be explained by the upper limb activities of daily life (ADL) often requiring greater ranges of motion in multiple planes to perform different tasks like grasping and reaching.[46] In contrast, during many gait activities, the requirement for a larger ROM is predominantly in the sagittal plane.[47]

3.1.2. ROM

For ROM, two different values could be considered, the overall ROM and the ROM required to meet the demands of most tasks. The overall ROM is the maximum value that a joint can reach in a plane. In contrast, the activity ROM is the ROM needed to perform a specific activity, which can be much less than the whole ROM of the joint (Table 1–7).

Therefore, in SWRR development, it is essential to know the ROM requirements for the tasks to be assisted.[46,47] As the AMSM is starting the developmental phase, it is reasonable to focus on specific and uncomplicated tasks.[48] With this in mind, it may be easier to develop simple robots that can achieve the practical demands of the patient.[49] For example, consider the hip joint in the sagittal plane during flexion–extension movement. The full ROM is from ≈120° flexion to ≈20° extension. Yet, during walking, the required range would be ≈40° flexion to 11° extension.

3.1.3. Joint Forces and Torques

For AMSM to generate the ROM sufficient to undertake tasks often performed in daily living, it must be able to generate sufficient forces/torques. These forces need to overcome those associated with gravity and the inertia of the limb being moved. In most research in this area, the reported value was torque.

Table 1. Shoulder Soft Wearable Robots Biomechanical Properties.

Research group	Material	DOF	ROM [°]	Torque/Force	Frequency	Angular velocity [° s^{-1}]	Control strategy	Weight [kg]
Human Body[34,51,139,140]	Skeletal muscle	3	Typical values −60 to 180 Extension/ Flexion 0 to 180 Adduction/ Abduction	Minimum to lift the patient's limb against gravity 79.9 Nm Flexion 74.9 Nm Extension 73 Abduction 76.4 Adduction	Typical values <20 Hz	Typical values >50	N/A	N/A
			ADLs −18.3 to 62.3 Extension/ Flexion −14 to 133.6 Adduction/ Abduction	ADLs 9.6 Extension/Flexion 10.05 Adduction/ Abduction	ADLs ≈1.1 Hz	ADLs 100 Extension/ Flexion 171.5 Adduction/ Abduction		
KAIST[100]	SMA (spring)	1	90 Abduction	10.1 Nm	N/A	18	N/A	0.675 Wearable assembly

Table 2. Elbow soft wearable Robots Biomechanical Properties.

Research group	Material	DOF	ROM [°]	Torque/Force	Frequency	Angular velocity [° s^{-1}]	Control strategy	Weight [kg]
Human Body[34,46,50–52,141]	Skeletal muscle	3	Typical values 0 to 150 Flexion/Extension −120 to 120 Pronation/Supination	Minimum to lift the patient's limb against gravity ≈3.5 Nm Flexion/Extension ≈1.85 Nm Pronation/Supination	Typical values <20 Hz	Typical values >50	N/A	N/A
			ADLs >81 Flexion/Extension −13 to 53 Pronation/Supination	ADLs ≈3.7 Nm Flexion/Extension ≈0.04 Nm Pronation/Supination	ADLs ≈1.25 Hz	ADLs <135 Flexion/Extension <486 Pronation/Supination		
University of Delaware[a)][60]	DEA	1	19.5	1 N (applied) weight applied to the arm	N/A	16.2	Pulse train	N/A
Carlos III University of Madrid[52]	SMA	2	0 to 120 Flexion/Extension −50 to 50 Pronation/Supination	3.5 Nm Flexion/Extension 1 Nm Pronation/Supination	100° at 0.2 rad s^{-1} (0.0318 Hz)	N/A	BPID	<1 (2.9 with power supply)
KAIST[97]	SMA (spring)	2	60 to 150 Flexion −27.6 to 27.6 Pronation/Supination	3.2 Nm Flexion/Extension 0.5 Nm Pronation/Supination	N/A	Full movement in 10 s	Step signal	1.55 Wearable assembly
Korea Institute of Machinery and Materials[101]	SMA (spring)	1	Strain of 26.1% (47 mm contraction)	80 N	N/A	Full movement in ≈5 s (With a cooling system and an agonist–antagonist configuration)	Step signal	0.57 Total

[a)]Biomechanical Properties based on children 2 years old.

Table 3. Wrist soft wearable Robots Biomechanical Properties.

Research group	Material	DOF	ROM [°]	Torque/Force	Frequency	Angular velocity [° s^{-1}]	Control strategy	Weight [kg]
Human Body[34,46,50,51,142]	Skeletal muscle	2	Typical values −38 to 40 Flexion/Extension −38 to 28 Ulnar deviation/Radial deviation	Minimum to lift the patient's limb against gravity 1.43 Nm Flexion/Extension 1.43 Nm Ulnar deviation/Radial deviation	Typical values <20 Hz	Typical values >50	N/A	N/A
			ADLs −38 to 40 Flexion/Extension −38 to 28 Ulnar deviation/Radial deviation	ADLs ≈0.2 Nm Flexion/Extension ≈0.3 Nm Ulnar deviation/Radial deviation	ADLs 1–5 Hz	ADLs <232 Flexion/Extension <203 Ulnar deviation/Radial deviation		
MENRVA[81]	TCP	1	N/A	0.3 Nm	≈13 N at 0.1 Hz	N/A	PID	N/A
Carlos III University of Madrid[94]	SMA	2	80 Flexion/Extension −45 to 45 Ulnar deviation/Radial deviation	0.5 Nm in both directions	50° at < 0.04 Hz Extension 40° at ≈0.04 Hz Ulnar deviation/Radial deviation	N/A	BPID	0.960 Total
KAIST[98]	SMA (spring)	2	−33.8 to 30.4 Flexion/Extension 21.4 to 15.4 Ulnar deviation/Radial deviation	1.32 Nm Extension 0.61 Nm Flexion 0.90 Nm Radial deviation 0.62 Nm Ulnar deviation	80° at 0.5 Hz	N/A	Step signal	0.151 Wearable assembly (Whole device ≈1)

Table 4. Hand (fingers) soft wearable Robots Biomechanical Properties.

Research group	Material	DOF	ROM [°]	Torque/Force	Frequency	Angular velocity [° s^{-1}]	Control strategy	Weight [kg]
Human Body[34,143,144]	Skeletal muscle	3 DOF Each finger	Typical values Index finger DIP = 70 PIP = 100 MCP = 90	Pinch of 1.4 N to 31.4 N	Typical values <20 Hz ADLs >1 Hz	Typical values >50	N/A	N/A
University of Pisa[68]	DEA	1	N/A	1 N	N/A	N/A	Step signal	N/A
Bio-robotics and Smart Systems Laboratory[59]	TCP	3 DOF Each finger	Index finger DIP = 11 PIP = 21 MCP = 41	2 N	N/A	Full movement in 25 s (Pulsed 2 s)	Step signal/ Pulsed actuation	≈0.1 Wearable assembly
Universidad Iberoamericana[82]	TCP	1	N/A	3 N	N/A	N/A	Step signal	N/A

Table 5. Hip soft wearable Robots Biomechanical Properties.

Research group	Material	DOF	ROM [°]	Torque/Force	Frequency	Angular velocity [° s^{-1}]	Control strategy	Weight [kg]
Human Body[34,145–148]	Skeletal muscle	3	Typical values −122 to 22 Flexion/ Extension −44 to 26 Abduction/ Adduction −33 to 34 Median rotation/Lateral rotation	Minimum torque to lift the patient's limb against gravity 80 Nm (120° flexion) ≈10 Nm (40° Flexion)	Typical values <20 Hz	Typical values >50	N/A	N/A
			ADLs −37.8 to 10.5 Flexion/ Extension −9.7 to 6.9 Adduction/ Abduction −1.0 to 11.2 Median rotation/Lateral rotation	Walking 80 Nm Flexion 65 Nm Extension 111 Nm Abduction 68 Nm Adduction 13 Nm Internal rotation 18.35 Nm External rotation	ADLs > 1.05 Hz	Walking <115 Extension <195 Flexion		
Zhejiang University of Technology[61]	PVC	1	N/A	≈70 Nm Flexion	N/A	N/A	State machine	0.6 Wearable assembly and 0.8 for the controller and the battery

However, for the hand, some devices have been developed to replicate/generate the force required for grasping and pinch activities. In the case of facial expressions, as with the finger joint, it is not measured on torque but the force that muscles generate in a direction to generate facial expressions.

Regarding torques, as with ROM, two different values are most often considered by developers. First, torque levels occur during ADLs and the minimum torque that would move the limb against gravity. Interestingly, the ADLs torques are similar or less for many activities in the upper limbs than the passive torques. For example, considering the wrist in ADLs, the necessary torques were less than 1 Nm in all directions, but in the case of torque required to move it against gravity, they were in the order of 1.5 Nm.[50–52] In contrast, in the lower limb, some muscles need to activate to a sufficient level to carry the person's body weight in the stance phase of gait activities and, at the same time, generate appropriate torque to produce the joint motion required for the gait activity being performed. For instance, the bigger discrepancy occurs during ankle plantarflexion, where a peak torque above 100 Nm is required, while for passive movement, the required torque is around 5 Nm.[53,54]

Table 6. Knee soft wearable Robots Biomechanical Properties.

Research group	Material	DOF	ROM [°]	Torque/Force	Frequency	Angular velocity [° s^{-1}]	Control strategy	Weight [kg]
Human Body[55,146,148,149]	Skeletal muscle	1	Typical values −134 to 1 Flexion/ Extension	Passive torque ≈50 Nm (≈50°)	Typical values <20 Hz	Typical values >50	N/A	N/A
			Walking −64.6 to 0 Flexion/ Extension	Walking 45.15 Nm	ADLs ≈1.15 Hz	Walking ≈360 Extension ≈300 Flexion		
Wyss Institute[a)][93]	SMA (spring)	1	−34 to 0 Flexion	N/A	N/A	2.56	Step signal	N/A

[a)]Biomechanical Properties based on children 4 years old.

Table 7. Ankle soft wearable Robots Biomechanical Properties.

Research group	Material	DOF	ROM [°]	Torque/Force	Frequency	Angular velocity [° s^{-1}]	Control strategy	Weight [kg]
Human Body[47,53–55,148]	Skeletal muscle	3	Typical values −55 to 20 Plantarflexion/ Dorsiflexion −23 to 12 Inversion/ Eversion	Passive torque ≈5 Nm (10°) Dorsiflexion ≈5 Nm (30°) Plantarflexion	Typical values <20 Hz	Typical values >50	N/A	N/A
			Walking −20 to 10 Plantarflexion/ Dorsiflexion	Walking Plantarflexion ≈110 Nm	ADLs ≈1.75 Hz	Walking ≈310 Plantarflexion ≈190 Dorsiflexion		
CNR Institute for Energetics and Interphases at Lecco[89,150]	SMA	1	−5 to 20 Plantarflexion/ Dorsiflexion	15 N with a lever arm of 10 cm (Torque = 1.5 Nm)	N/A	N/A	Square pulse	N/A
State Key Laboratory of Mechanism System and Vibration[85]	SMA	1	−16 to 16 Plantarflexion/ Dorsiflexion	10.9 Nm	16° at 1 Hz	N/A	SBH Feedforward + PID	N/A
Ajou University[91,92]	SMA	1	20 Plantarflexion	1 Nm	N/A	100 contraction	Step signal	0.428 g Without power supply

Table 8. Facial soft wearable Robots Biomechanical Properties.

Research group	Material	DOF	Displacement	Torque/ Force	Frequency	Angular velocity [° s^{-1}]	Control strategy	Weight [kg]
Human Body[151]	Skeletal muscle	N/A	N/A	1.1–3.5 N	N/A	N/A	N/A	N/A
Artificial Intelligence Laboratory[88]	SMA	N/A	20 mm	N/A	N/A	N/A	Feedback controller	N/A

3.1.4. Frequency and Angular Velocity

Human movements are dynamic tasks, and therefore these are characterized by temporal parameters like angular velocity and frequency of the movements. Even if these are related to each other, these are different concepts, and ideally, both should be reported. Angular velocity is the rate of flexion and extension of a joint, while frequency is related to the maximum trackable sinusoidal frequency of the amplitude of the movement. It is possible to approximate the angular velocity from the frequency with the next formula.

$$\omega = \lambda * 2 * F \tag{1}$$

where ω is the angular velocity in $^\circ\,s^{-1}$, λ is the amplitude of the sinusoidal wave in °, and F is the frequency in Hz. In the case of the velocities, it is possible to notice that it varies depending on the extremity, from around $120^\circ\,s^{-1}$ in the case of the ankle to more than $400^\circ\,s^{-1}$ for the elbow (Table 1 and 7). However, in the case of the frequencies, they remain similar, around 1.5 Hz.[55] This could be related to the fact that speeds are not constant during the movement, while the frequencies are related to the median speed of a movement limited in a specific ROM. In the case of the SWRR, when the frequency is provided is essential to look at the amplitude to estimate how fast a device is.

3.1.5. Control Strategies

The control strategy is a crucial element during the design process of SWRR. The control strategy's objective is to track the device's trajectory[56] and/or forces[57] to plan the desired action to apply a stimulus to the actuator later to generate a movement. This process is similar to the motor control of the human body, where the central nervous system plans the movement base on sensory information and sends the command to drive the muscles.[58] From the founded devices, it is possible to identify mainly three different control strategies, pulses, state machines, and proportional–integral–derivative (PID) controllers.

The pulse strategy is an open-loop control strategy as the system's output depends on the input, but the input is independent of the output. This scheme consists of applying a pulse or steps to generate a certain level of force or displacement from the AMSM. However, there is no feedback. Thus, it is impossible to compensate for the influence of external stimuli.[59,60]

In the case of the state machine, the device can change between different states in response to an event. The simple state machine is an on–off switch that changes based on an external stimulus, such as the change between the gait swing and stance phases.[61]

PID is a closed-loop control mechanism employing feedback from the system output. The controller is continuously calculating an error value between the reference signal and the output and then applies a correction. PIDs are used to reject disturbances and to implement setpoint changes.[52]

3.1.6. Weight

The weight of the artificial muscle and overall device is critical to establishing its usability by patients. Excessive weight can negatively affect the motion of the limbs as significant weight generates inertial forces that increase energy consumption and could make it uncomfortable and unsafe for patients to use.[62] For instance, the threshold for an acceptable weight on the hand and forearm is around 400 to 500 g.[63] Furthermore, in the case of the lower limbs, a weight of 4 kg on foot doesn't seem to affect the gait kinematics. However, the net metabolic rate increased by 36%.[64]

3.2. Soft Wearable Rehabilitation Robots

While biomechanical considerations are the main factors to consider in the design of SWRR, the system's capabilities depend more on the functional properties of the AMSM that are inherited from the material used to fabricate them. In this section, the different systems are presented and arranged by the material used to manufacture them. In this section, the different systems are presented and arranged by the material used to manufacture them to understand the advantages and disadvantages of each AMSM technology applied to SWRR.

Table 1–8 present the material utilized, the system's weight, the control strategy, the ROM at the joint involved, frequency of motion, typical joint angular velocities, and the associated torques. These parameters are presented within subsections related to body parts upon which systems were designed.

3.2.1. DEAs

EAPs are polymers that can be stimulated to change their shape using electrical energy. One of the most common types of EAPs is DEA.[65] It consists of a compliant capacitor composed of a thin elastic dielectric film coated on both surfaces by compliant electrodes. When DC voltage is applied to the electrodes, both attract each other, increasing the pressure over the dielectric film (Maxwell pressure) due to the electrostatic force while reducing thickness and area expansion (**Figure 3**).[39,66] Maxwell pressure is related to the permittivity of the material and the strength of the applied electric field. The relation can be expressed as

$$P = \varepsilon_0 \varepsilon_m E^2 = \varepsilon_0 \varepsilon_m (V/d)^2 \quad (2)$$

where P is the Maxwell pressure, ε_0 is the vacuum permittivity, ε_m is the material permittivity, E is the electric field strength that depends on the applied voltage V, and the thickness of the film d. *DEAs in Wearables Devices*: DEA actuators are one of the most studied AMSMs due to their properties that, in most cases, surpass those of the muscle, with strain approaching 200%, a high bandwidth up to the range of kilohertz, and high efficiency,[33,34,67] which are all desirable properties for SWRR. However, they have limitations when placed in robotic applications that interact with people. DEAs need high voltage, in the order of hundreds of volts, requires bulky and expensive electronics and are considered unsafe. Nevertheless, DEAs are challenging to produce in a compact size to generate appropriate amounts of power and force.[18,66]

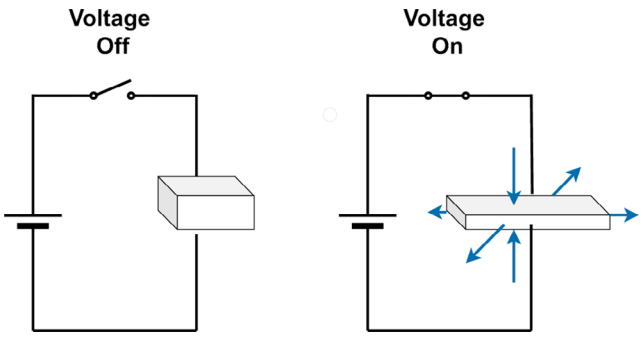

Figure 3. The working principle of the DEAs, when a voltage is applied, a Maxwell pressure is generated between the electrodes.

Two different research groups developed SWRR with this AMSM. Carpi et al.[68] developed a hand rehabilitation device based on folded DEAs to generate flexion and extension movements at the finger joints actively. The structure of the hand-split consists of a plastic-made wrist guard with support for the actuator in combination with an aluminum rod. Three folded DEAs actuators were connected to a miniature DC to high-voltage DC converter to provide the required high voltage. The converters were able to supply voltage in the range of 0–10 kV. With this configuration, the device could generate forces in a range of 1 N and a contraction of 7% to the original length using an input voltage ranging from 0 to 6 kV.

Behboodi et al.[60] designed a platform for pediatric rehabilitation to generate flexion and extension movements of the elbow joint (**Figure 4**). The device used a bundle of stacked DEAs,[66] with three parallel fibers consisting of 5 stacked DEAs in series.

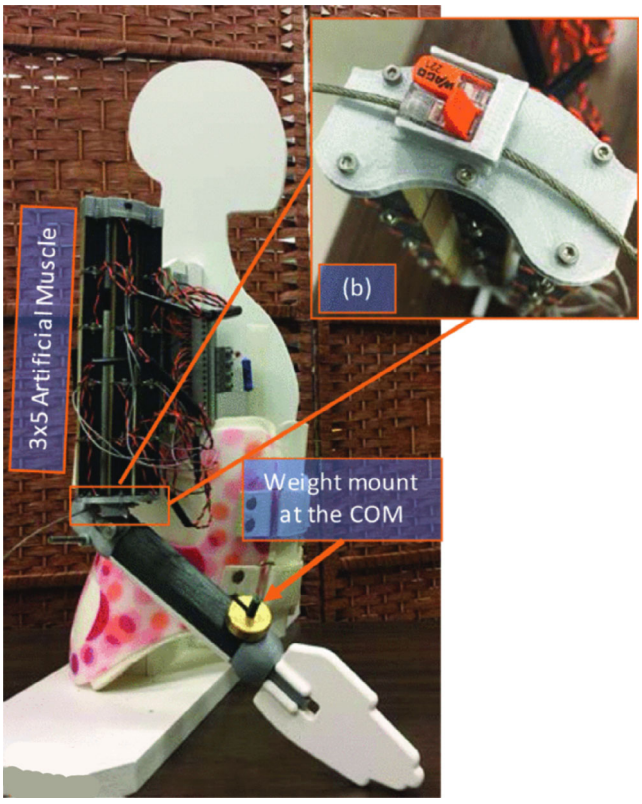

Figure 4. Example of a SWRR based on DEAs. Reproduced under the terms of the CC BY license.[60] Copyright 2020, IEEE.

The bundle of actuators was mounted on a mannequin resembling the elbow joint of a 2 years old child, and it was able to flex the elbow at 19.5° with an angular velocity of 16.2° s^{-1}. These results were obtained by applying a square signal with 1230 V amplitude.

3.2.2. PVC Gel Actuators

PVC gel actuators are EAPs similar to DEAs. PVC gels are produced by thermally or chemically melting PVC resins with liquid plasticizers. When PVC gel is placed between electrodes and an electric field is applied, a creeping deformation on the anode can be observed, and when the electric field is discharged, the PVC gel returns to its original shape[69,70] (**Figure 5**). The creep deformation can generate different types of deformation like bending, crawling, and linear contractions.[71]

Hashimoto et al.[72] developed an AMSM from PVC gel able to generate contractions. The PVC gel was sandwiched between a stainless mesh that acted as an anode, while a stainless foil served as a cathode. The cathode was located under the PVC gel, and the anode was above the gel. When the electric field is applied, the PVC gel creeps up the anode and moves into the mesh. The PVC electro-mechanical dynamics can be modeled as

$$\frac{\alpha}{T_\alpha s+1} * \frac{1}{R_1 R_2 C s + R_1 + R_2} E(s) = \beta X(s) + F_{\text{ext}}(s) \tag{3}$$

where $X(s)$ and $F_{\text{ext}}(s)$ are the contraction strain and output stress, respectively. $E(s)$ is the applied electric field. The terms R_1, R_2, and C are the resistances and capacitance from an equivalent electric circuit. T_α is the time constant of the system. α and β are gains that can be determined from the experimental results.

PVC Gels in Wearable Devices: PVC gel actuators are a promising technology to be used as AMSM for SWRR, with their main advantages being relatively high actuation frequency (about 9 Hz), high strain (75%), low power consumption (2.9 μW mm^{-2}), and a very long life span (>5 million cycles). However, they require high voltages to work (≈3600 V), have low stress (0.6 MPa), and additionally, the electromechanical deformation mechanism is not fully understood, making it challenging to generate controlled joint movement.[61,71]

Only one SWRR has used this technology (**Figure 6**). Yi Li and Minoru Hashimoto are pioneers in using PVC gel actuators for wearable devices. In 2015, they presented their first prototype of a wearable system to assist in hip joint motion while walking.[73] Their latest development has been to upgrade the system with a new actuation unit.[61] The actuation unit had a length of

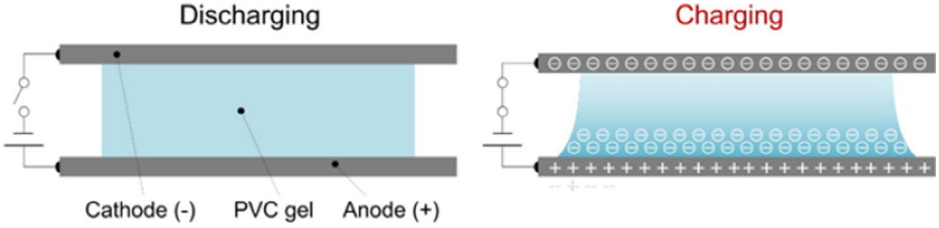

Figure 5. Deformation mechanism of polyvinyl chloride (PVC) gel when an electrical stimulus is applied. Reproduced under the terms of the CC BY license.[70] Copyright 2015, The Authors. Licensee InTech.

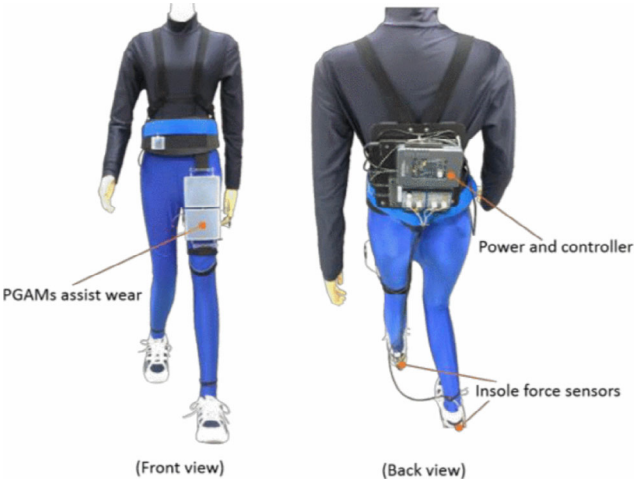

Figure 6. Example of an SWRR based on PVC gel actuator. Reproduced with permission.[138] Copyright 2016, IEEE.

200 mm, and to ensure appropriate fitting to the human body, it had a curved shape to mold more accurately to the body part. The whole device (for two legs) weighed 2 kg (0.6 per actuation unit + 0.8 kg for the control unit, including the battery). When the whole system was tested using a voltage of 400 V, the displacement of the assistive device was ≈16 mm (8%), the maximum output force was around 94 N, the response time was ≈56 ms, and the power consumption was around 1.6 W. The device was activated through a state machine controller strategy, switching the assistance on and off during the swinging and stance phase, respectively.

3.2.3. TCP Actuators

TCP actuators have emerged as a promising AMSM technology for SWRR. TCP actuators are constructed by continuously twisting polymer fibers or filaments (e.g., nylon fishing lines and sewing threads) until they form coils. The actuator works by converting a temperature change into strain or stress. In general, TCP actuators are driven by Joule heating (**Figure 7**a), adding a layer of a conductive material (e.g., silver) over the precursor fiber[74,75] or by embedding a resistance wire within the actuator[76,77] (Figure 7b). Consequently, the actuator can be modeled as an electrothermal–mechanical system. The electrothermal dynamics can be represented as a first-order linear system represented as[78,79]

$$C_{\text{th}}\frac{dT}{dt} = P(t) - \lambda(T - T_0) \tag{4}$$

where C_{th} and λ are the actuator's thermal mass and absolute thermal conductivity, respectively. T is the actuator's temperature, T_0 is the ambient temperature, and $P(t)$ is the electrical input applied at a specific time t. To quantify the speed of the dynamics, the time constant, $\tau = \frac{C_{\text{th}}}{\lambda}$ can be adopted. τ can be obtained by examining the actuators' rise and fall response and is equal to the average time the actuator takes to reach the 63% of a steady-state value given a step input under a steady-state condition.

In the case of the thermomechanical properties, this can be described as a spring–damper system with an added temperature-dependent term, which is expressed as

$$F = k(x - x_0) + b\dot{x} + c(T - T_0) \tag{5}$$

where x and x_0 are the loaded lengths and resting lengths of the actuator, respectively. K represents the stiffness, b is a damping term, and c denotes the thermal constant. Under steady conditions where $\dot{x} = 0$, the overall model can be obtained by combining (3) and (4).

$$F = k(x - x_0) + \frac{c}{\lambda}P \tag{6}$$

TCPs in Wearables Devices: TCPs are a recent discovery.[80] They have gained significant attention in the field of SWRR, with advantages such as high-power density (27 W g^{-1}) and stress (10 MPa), linear behavior, and a high strain (21%). In contrast, their main disadvantages are low efficiency (≈1%)[28,33,34] and the low frequencies (<3 Hz) at which they operate. Three promising examples of wearable devices based on TCPs were found.

The assistive wrist orthosis developed by Sutton et al.[81] used an arrangement of 16 TCPs wires made of silver-coated Nylon 6.6 sewing thread (**Figure 8**a). The splint prototype consisted of 3D-printed parts to mount the device on the arm and attachments for

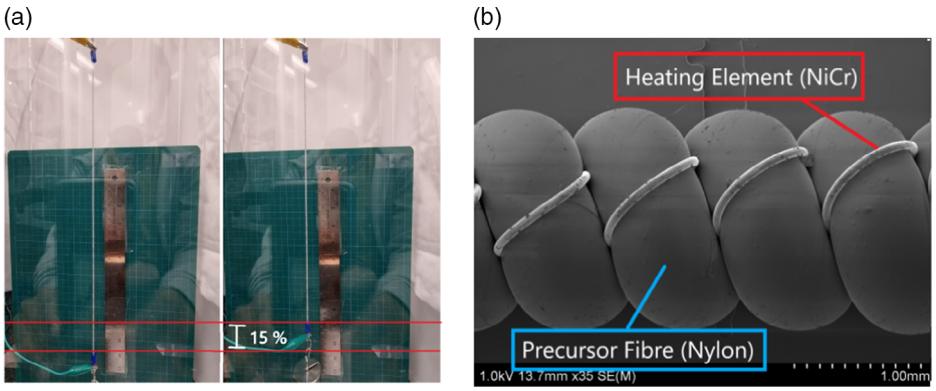

Figure 7. a) TCP actuator lifting a 1 kg load by 15% strain after heat is applied. b) Scanning electron microscope image of a nylon TCP actuator with a NiCr embedded wire as the heating element.

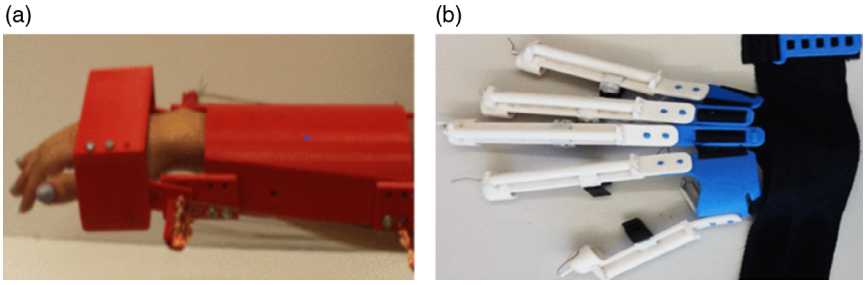

Figure 8. Examples of SWRR based on TCP are: a) MENRVA group SWRR for wrist. Reproduced with permission.[81] Copyright 2016, IEEE. b) Universidad Iberoamericana SWRR for hand. Reproduced with permission.[82] Copyright 2018, IEEE.

the nylon actuators. The device was designed to have one DOF and provide a torque of 0.3 Nm on the wrist joint in the flexion direction. The final prototype was able to produce torques around 0.32 Nm in 3.9 s. Using a PID controller, the system could track a 0.1 Hz with an amplitude of 10 N during actuation very closely, but during the relaxation time, the error increased due to the slow response time during the cooling down phase.

The group of Saharan et al.[59] designed iGrab, an ergonomic orthotic device powered by TCPs, to assist flexion and extension movement of the fingers. The prototype comprised 3D printed parts and sewn parts with artificial tendons routed from the fingers to the wrist using polytetrafluoroethylene (PTFE) pipes. The tendons were connected with a metallic ring to the TCPs mounted on a forearm bracelet. The TCP muscles were wrapped around frictionless pulleys to utilize long actuators. Furthermore, to improve energy consumption, the extension motion was facilitated with the help of rubber strips. When a 0.6 A step signal was applied to the TCPs, the fingers were able to reach their maximum displacement after 25 s (i.e., the index finger was able to move 40° for the MCP joint, 21° for the PIP joint, and 11° in the case of the DIP joint). The results were improved when a pulsed signal was used, reducing the actuation time from 25 s to less than 5 s.

Patiño et al.[82] also developed a wearable orthosis for hand rehabilitation movements, with a TCP actuator on each finger (Figure 8b). The exoskeleton is composed of two main parts fitted to the dorsum of the hand and the fingers. The dorsum of the hand was composed of five 3D printed plates, of which four are aligned with the fingers and one more adjustable plate that serves to fit the device to the user's hand. In the case of the fingers, each of them is composed of a silicone tube containing a TCP and a filament strain sensor. The TCP inside the finger structure could produce forces of around 3 N when a step input of 0.3 A was applied.

3.2.4. SMAs

SMAs are metallic materials that use the memory effect property to generate motion. The SMP is defined as the material's property to recover a previously described shape when an external stimulus is applied. Nickel–titanium (NiTi) alloys are the most popular SMAs, and they recover their original "memorized" shape after being deformed when heated above their transformation temperature.[38,83] SMA can be used as single fibers (**Figure 9**a) or as springs (Figure 9b) to generate linear displacement. SMA elements are generally heated through the Joule effect, where an electric current is applied to the SMA actuator. However, they present a high thermal hysteresis between the transition that occurs from martensite (low temperatures) to austenite (high temperatures) and the one occurring from austenite to martensite[84] (Figure 9c). When using a model is essential to take into consideration the nonlinear hysteresis properties of the material as the system's behavior in both phases is different.[85,86]

Zhang et al.[85] propose a sigmoid-based hysteresis (SBH) model for a single SMA fiber, where they introduce two different sigmoidal curves representing the major hysteresis properties.

$$y = \frac{k(\sigma,f)}{1+e^{-a_+(\sigma,f)[u-r_+(\sigma,f)]}} \quad \text{For } \dot{u} \geq 0 \tag{7}$$

$$y = \frac{k(\sigma,f)}{1+e^{-a_-(\sigma,f)[u-r_-(\sigma,f)]}} \quad \text{For } \dot{u} < 0 \tag{8}$$

where u is the input voltage, y is the output displacement. k represents maximum displacement. σ signifies the prestress applied to the fiber. f denotes the driving frequency. $a_{+/-}$ and $r_{+/-}$ represent curve slopes and voltage values at peak transformation of martensite to austenite and austenite to martensite. Besides, the hysteresis gap can be represented by $\Delta r(\sigma,f)$, which is defined as follows

$$\Delta r(\sigma,f) = r_+(\sigma,f) - r_-(\sigma,f) \tag{9}$$

To compensate for the minor hysteresis properties, two suitable scaling factors $\beta_{+/-}$ (where $\beta_{+/-} \in [0,1]$) are introduced. Hence Equation (7) and (8) can be rewritten as

$$y = \beta_+ \frac{k(\sigma,f)}{1+e^{-a_+(\sigma,f)[u-r_+(\sigma,f)]}} \quad \text{For } \dot{u} \geq 0 \tag{10}$$

$$y = \beta_- \frac{k(\sigma,f)}{1+e^{-a_-(\sigma,f)[u-r_-(\sigma,f)]}} + (1-\beta_-)k(\sigma,f) \quad \text{For } \dot{u} < 0 \tag{11}$$

For SMA springs, Koh[111] introduced a model derived by combining the conventional coil spring equation and a large deformation term for the austenite (12) and martensite (13) phases, respectively.

$$F_A = \frac{G_A d^4}{8D^3 n}\left(\frac{\cos^3\alpha_i}{\cos^2\alpha_{AF}(\cos^2\alpha_{AF} + \sin^2\alpha_{AF}/(1+\nu))}\right)\delta_A \tag{12}$$

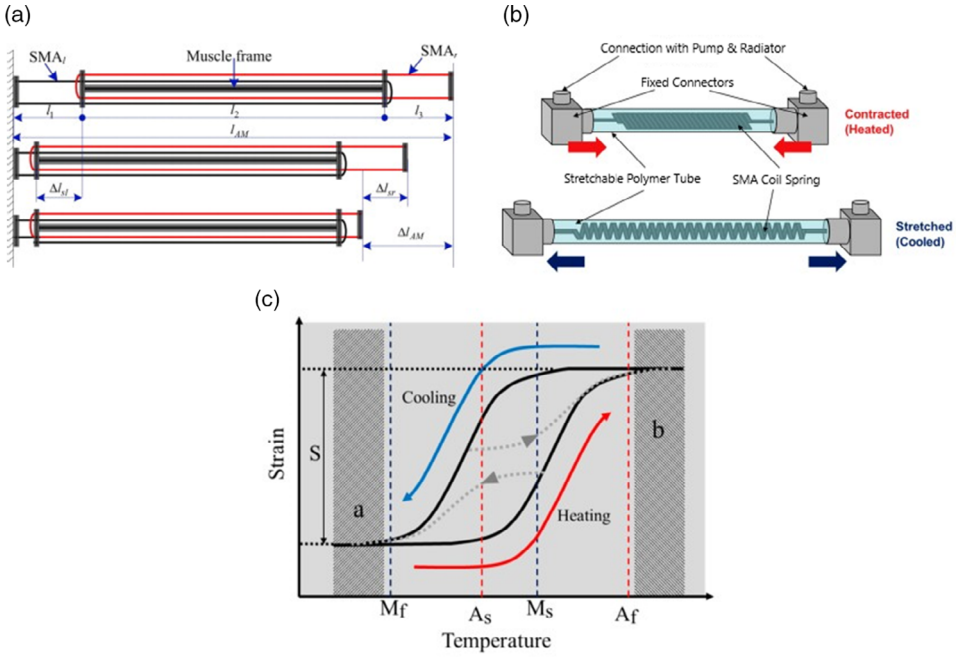

Figure 9. SMA actuators were functioning after and before applying joule heating. As: a) wires or b) springs. a) Reproduced with permission.[85] Copyright 2013, Elsevier. b) Reproduced under the terms of the CC BY license.[98] Copyright 2019, The Authors. Licensee MDPI. c) Temperature strain relationship of SMA actuators (As = Austenite start, Af = Austenite finish, Ms = Martensite start, Mf = Martensite finish). Reproduced under the terms of the CC BY license.[86] Copyright 2018, The Author. Licensee MDPI.

$$F_{\mathrm{M}} = \frac{G_{\mathrm{A}} d^4}{8D^3 n}\left(\frac{\cos^3\alpha_i}{\cos^2\alpha_{\mathrm{MF}}(\cos^2\alpha_{\mathrm{MF}} + \sin^2\alpha_{\mathrm{MF}}/(1+\nu))}\right)\delta_{\mathrm{M}} - \frac{\pi d^3}{8D} G_{\mathrm{M}}\gamma_{\mathrm{L}}\xi_{\mathrm{S}\gamma} \tag{13}$$

where the material properties are: G the shear modulus, ν the Poisson's ratio, and γ_{L} the residual strain. Then the design parameters determined by the user are: d wire diameter, D the coil diameter, α_i initial pitch angle, and n the number of the coils. Lastly, the variables are F the force, $\xi_{\mathrm{S}\gamma}$ the detwinned martensite volume fraction that changes with temperature and stress, δ the displacement, and αf the final pitch angle. Subscripts A and M denote the austenite and the martensite, respectively.

The deformation of the coil can be represented with δ, αf, γ. Although these variables are dependent variables, combining them complicates the equations. The pitch angle α_{f} is the term that describes the large deformation of the spring, δ is the original spring force–displacement, and γ is the shear strain for the detwinning term. Equations to describe the relationship of these three variables are provided so that they can be converted as needed. α_{f} can be converted to δ with Equation (14). Also, the final pitch angle can be converted to γ with Equation (15).

$$\delta = \frac{\pi n D}{\cos\alpha_i}(\sin\alpha_{\mathrm{f}} - \sin\alpha_i) \tag{14}$$

$$\gamma = \frac{d}{D}\frac{\cos^2\alpha_i(\sin\alpha_{\mathrm{f}} + \sin\alpha_i)}{\cos^2\alpha_{\mathrm{f}}(\cos^2\alpha_{\mathrm{f}} + \frac{\sin^2\alpha_{\mathrm{f}}}{1+\nu})} \tag{15}$$

Furthermore, F can be converted to τ with Equation (16).

$$\tau = \frac{8DF}{\pi d^3} \tag{16}$$

The detwinned martensite volume fraction ($\xi_{\mathrm{S}\gamma}$) is commonly a function of τ and temperature. However, to simplify the model $\xi_{\mathrm{S}\gamma}$ is modified to be a function of γ as follows.

$$\xi_{\mathrm{S}\gamma} = \frac{1}{2}\cos\left(\frac{\pi}{\gamma_{\mathrm{s}}^{\mathrm{cr}} - \gamma_{\mathrm{f}}^{\mathrm{cr}}}(\gamma - \gamma_{\mathrm{f}}^{\mathrm{cr}})\right) \tag{17}$$

where γ^{cr} is the critical strain for detwinning start ($\gamma_{\mathrm{s}}^{\mathrm{cr}}$) and finish $\gamma_{\mathrm{f}}^{\mathrm{cr}}$, which is the property of SMA.

In summarizing, Equation (12) and (14) are used to plot the force–displacement relationship for the full austenite phase, and Equation (13)–(15),(17) are used to plot the force–displacement relationship for the full martensite phase. Equation (14)–(16) are used to convert the force–displacement relationship into a shear stress and shear strain relationship.

SMAs in Wearables Devices: SMAs are superior to mammals' muscles and other AMSMs in terms of power density and stress, these being as high as $50\,\mathrm{W\,g^{-1}}$ and 200 MPa, respectively. Consequently, SMA actuators have been successfully used in automotive, aerospace, and biomedical fields.[87] However, they have limitations in respect of robotic rehabilitation, and these are low efficiency, a small strain range (up to 8%), and high thermal hysteresis making them difficult to control.[18,33,34] Nevertheless, SMA is the most used AMSM for rehabilitation robots, and it has been used within nine different devices.

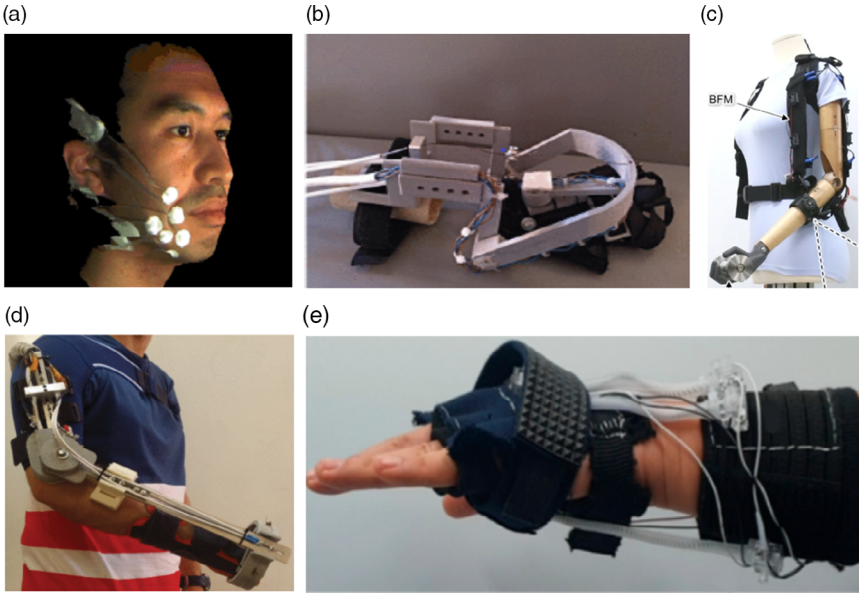

Figure 10. Examples of SMA-based SWRR. a) Artificial Intelligence Laboratory Smile recovery device. Reproduced with permission.[88] Copyright 2008, IEEE. b) Carlos III University of Madrid wrist device. Reproduced with permission.[94] Copyright 2018, IEEE. c) Korea Institute of Machinery and Materials elbow robot. Reproduced under the terms of the CC BY license.[101] Copyright 2022, The Authors, published by Springer Nature. d) Carlos III University of Madrid elbow SWRR. Reproduced under the terms of the CC BY license.[52] Copyright 2019, IEEE. e) KAIST Wrist SWRR. Reproduced under the terms of the CC BY license.[98] Copyright 2019, The Authors. Licensee MDPI.

Jayatilake et al.[88] investigated the ability of a device based on spring SMAs to help people with facial paralysis recover the ability to make facial expressions (**Figure 10**a). The device consisted of a wearable robotic external mask. The mask included six SMAs per side, and these were arranged in a specific position to replace or reproduce the face muscles' activity. The authors reported that it was possible to generate some facial expressions with a contraction of 20 mm, using a feedback controller. However, to create complex facial expressions, several SMAs are required.

Pittaccio et al.[89,90] developed SHADE, an ankle orthosis capable of providing active and passive exercise for the dorsiflexion movement. The system used an SMA wire mounted on an insulated aluminum cartridge with dimensions of $150 \times 20 \times 15$ mm. Inside the cartridge, the wire was led back and forth between two arrays of ten mini-pulleys, making it possible to store a long wire within a limited space. The prototype consisted of two cartridges and two thermoplastic shells hinged at the ankle joint. Later, three adult patients tested the prototype. During these trials, the prototype provided passive dorsiflexion movements in the range of 0–23° to all the patients with speeds similar to the movement's natural speed. The control signal used during the experiments was a square signal with a current injection of 0.7 A for 7 s and a coiling phase of 30 s.

Zhang et al.[85] proposed using SMAs on an SWRR to assist the ankle dorsiflexion movement. To power the SWRR, an actuation unit composed of 2×250 mm SMA wires were developed. The system consisted of two parallel units and a bias spring mounted in two lightweight thermoplastic shells with articulated joints. To compensate for the hysteresis of the SMA, the prototype employed an SBH feedforward controller with a PID controller. With this control configuration, the system was tested by following a sinusoidal signal with a peak-to-peak value of 30° at 0.2 Hz and 16° at 1 Hz. The system tracked the signal with a maximum tracking error lower than 16% and the root-mean-square tracking error lower than 7.3% in both cases.

Regarding plantarflexion at the ankle joint, Koo et al.[91,92] produced a lower extremity SWRR using SMA wire. The system was light, silent, and flexible. A prototype was built using a multilayered structure consisting of functional fabrics, seam sealing tape, Velcro straps, Teflon tubes, and an SMA cable. The SMA was wrapped around the lower limb with both ends of the SMA anchored at the waist, and the middle part of the cable was attached to the ankle. The viability of the prototype was evaluated using an adult-like PVC mannequin. Joule heating was employed to activate the system, and when a 1 A current was applied, an angular displacement of around 20° (plantar flexion) within 0.2 s was achieved.

For the knee joint, Stirling et al.[93] investigated the use of spring SMA on an active soft orthotic (ASO) device. The ASO comprised four sets of actuators on the dorsal surface of the knee (to assist flexion) and one set on the frontal surface (to help extension). Each group of actuators consisted of four SMA springs with a length of 17.5 cm. The system was tested on a robotic leg resembling the size and mass of that of a 4 years old child. With the four sets of actuators activated through joule heating, the ASO flexed the knee by 34° in ≈25 s. The results were obtained after applying a step signal of 0.4 A to each set of actuators.

The Carlos III University of Madrid group has published a number of articles concerning SWRR actuated by SMA.[52,83,94–96] Recently, a wrist rehabilitation robot[94] was

designed to assist flexion, extension, ulnar deviation, and radial deviation movement (Figure 10b). The rehabilitation robot consisted of a 3D-printed mechanical structure sewn onto a glove. The device used three SMA wires, one for the extension movement and a pair to generate the ulnar/radial deviation movements. A sinusoidal signal with a frequency of 0.04 Hz and a ROM of −10° to 40° was used to test the flexion–extension and the radial–ulnar deviation movements. The SWRR was able to track the extension movement, but it could not follow the signal input during flexion due to the slow cooling process of SMA. In ulnar/radial deviation movement, it tracked the whole movement as it presented an agonist–antagonist structure, improving the performance compared to a single wire.

Another article from this research group concerned an elbow SWRR[52] (Figure 10d) that had two DOFs (flexion/extension and pronation/supination). Each DOF had a pair of antagonist SMA actuation units. The units utilized a set of SMA wires encapsulated inside a PTFE tube. The number of SMA wires inside the actuation unit differed according to the direction of the movement. In the case of the flexion–extension, the actuation units were configured with a bundle of three SMA wires 1.5 m in length for flexion and two for extension. For the pronation/supination movement, each direction was actuated by a single SMA wire with a length of 2 m. To test the device, a sinusoidal signal with an amplitude of 100° and a frequency of 0.2 rad s^{-1} was applied while performing a flexion–extension movement. The device could follow the pattern with an error of less than 4°. In both devices, to control the contraction of the SMA wires, they used a four-term bilinear-proportional–integral–derivative (BPID). The BPID controller is a combination of a standard linear PID controller cascaded with a bilinear compensator to counteract the hysteresis behavior of the SMA.

A group from the Korea Advanced Institute of Science and Technology (KAIST)[97–99] has designed SWRRs to assist patients who have difficulty moving the upper limb using SMA springs. The first SWRR they developed was a device to assist wrist movements[98,99] (Figure 10e). They chose to use single SMA springs to generate a high contraction strain. The SWRR consisted of a wearable fingerless glove worn on the hand and a wearable strap placed on the forearm. Five actuators were used to provide the required movements, three over the forearm and two under the forearm. A cooling system pumping mineral oil was employed to improve the speed of the SMA springs. The device could provide torques of 1.32, 0.61, and 0.90, and a 0.62 Nm for extension, flexion, radial deviation, and ulnar deviation movements. Regarding the ROM while the SWRR was worn, it was 33.8°, 30.4°, 21.4°, and 15.4° for flexion, extension, radial deviation, and ulnar deviation, respectively. To achieve a cycling performance of 0.5 Hz, a step signal of 4 A was applied to the SMA springs during the heating phase, while a step signal of 2.7 W was used for the pump during the cooling phase.

After the wrist device, the KAIST group developed two DOFs SWRR to assist during the elbow's flexion and pronation/supination movements.[97] The device used artificial muscle units composed of a bundle of four SMA springs inside of a coolant-based vessel containing mineral oil. The robot presents three different artificial muscle units attached to soft braces to mimic the motions of human muscles. One unit is used by itself to assist elbow flexion, while the other two are arranged in an agonist/antagonist structure to help with the forearm pronation/supination. The device was able to provide torques up to 3.2 Nm with a ROM in the range of 60° to 150° for flexion movement. Meanwhile, for the pronation/supination, the ROM was from −26.7° to 26.7° with a torque up to 0.5 Nm. The result from the forearm was obtained by applying a current of 1.5 A for 10 s in ambient temperature.

Finally, KAIST developed a four-bar linkage-based SWRR to assist with shoulder abduction.[100] An actuator was designed to generate the required forces using a bundle of 14 SMA springs. Each actuator produced an output force of 270 N when the actuator was stretched by up to 150%. The system consisted of a four-bar linkage-based supported hinge and an actuator unit. Where the four links are constructed by the arm, the torso, and two extra 100 and 200 mm connected linkages. Furthermore, the actuator was placed in the middle of the 200 mm link and the upper arm. With this configuration, the mechanism could produce assistive torque up to 10.1 Nm and a ROM of 90° during shoulder abduction. An electrical current of 1.5 A was supplied to each spring to activate the device. The effect of assistance was evaluated by measuring and analyzing the difference in the electromyography (EMG) activity between assisted and unassisted activity. However, there were no significant differences between the two conditions.

At the Korea Institute of Machinery and Materials, Park et al.[101,102] presented an SWRR made of fabric muscle with a cooling acceleration structure for elbow extension assistance (Figure 10c). The device is actuated by fabric muscle that consists of SMA spring bundles, conductive fabrics, cover fabrics, and electrical wiring. Furthermore, to improve the cooling rate of the fabric, two small fans are attached to each piece of fabric. The final exosuit consists of a shoulder anchor, forearm anchor, two overlapped biceps fabric muscles, one triceps fabric muscle, battery, and controller (with a total weight of 0.57 kg). The biceps fabric muscles were set on an agonists–antagonist configuration to improve the system's speed. Furthermore, when the fans were used, the system could contract 47 mm (26% strain) and generate a force of 80 N while flexing the elbow in 5 s. This was achieved by applying 10 A to the bicep's fabric for 3 s and fan cooling and activating the triceps fabric (10 A) for 3 s.

3.2.5. Other Smart Materials

While those materials presented earlier have been utilized for SWRR, there are other materials that had been highlighted as a possible option in previous articles,[37,103] like IPMC,[104] hydraulically amplified self-healing electrostatic (HASEL),[103] and SMP[105] that present attractive properties as they have been used in similar applications (grippers, robotic hands, or as compliance mechanism inside a rehabilitation robot). However, their current limitations prevent their use on SWRR.

IPMCs are EAPs made by coating a thin sheet of ionic polymer with metal electrodes. When an external electric field is applied, ions of the same charge begin to move from the anode to the cathode. As a result, the system undergoes a fast-bending deformation, followed by a slow relaxation[106,107] (**Figure 11**a). They have compelling advantages, such as efficiency, low working voltage (1–5 V), high working frequency up to 100 Hz, and

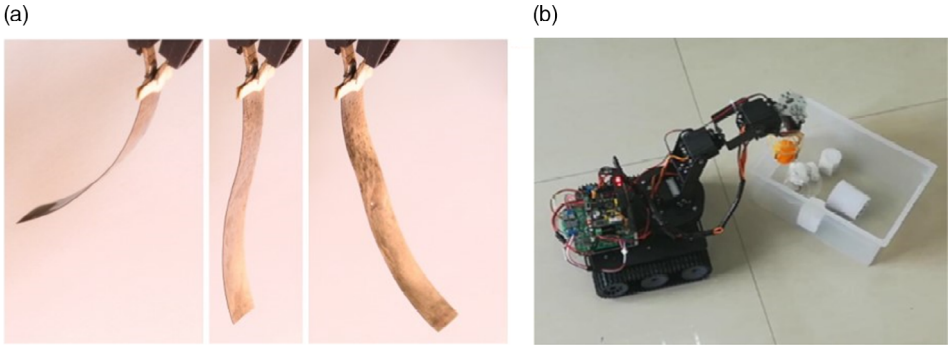

Figure 11. a) IPMC actuator bending in response to an electrical input with opposite polarities (left and right) and at rest (middle). Reproduced under the terms of the CC BY license.[107] Copyright 2019, The Authors. Licensee MDPI. b) Air-operating IPMC soft gripper assembled with a mobile mechanical arm. Reproduced with permission.[110] Copyright 2020, IOP.

considerable strain up to 40%. Nevertheless, they present some problems, such as relaxation under direct current (DC) voltage, low power density (0.02 W g^{-1}), and solvent evaporation that complicate their use in not watery environments.[33,108,109] He et al.[110] developed a microgripper using an air-operating IPMC actuator with consecutive channels. However, under this environment, the actuator by itself was only able to produce a strain of 0.44% and a force of 12.06 mN at 1 Hz using 5 V input which is lower than what skeletal muscles can generate. Nevertheless, the actuator proved its functionality operating on air, as it was used on a microgripper (0.14 g) that was able to pick up and transfer a nut (0.656 g) 4.69 times its own weight (Figure 11b).

Recently introduced HASEL actuators are fabricated from dielectric liquids filling pouches made of polymer films and partially covered by electrodes[111] (**Figure 12**a). HASEL actuators behave similarly to DEAs. They generate a Maxwell pressure when high voltage is applied, increasing the volume of the pouches and decreasing the length of the actuator.[112] Their main advantages for rehabilitation devices are their high linear strain (over 24%) and high bandwidth (126 Hz). Nevertheless, as with the DEAs, their main limitations are low stress (<1 MPa) and the high voltage (in the range of kV) required to drive them.[113] To understand the advantages and disadvantages of the HASEL actuator in rehabilitation robots, Yoder et al.[114] compared the HASEL actuator with DC motors, activating the Bebionic v2 Prosthetic hand (Figure 12b). In this comparison, the HASEL actuator surpassed the speed (HASEL = 1,587° s^{-1}, Motor = 150° s^{-1}) and the energy consumption (HASEL = 0.94 mW, Motor = 9,200 mW) of the motor. The ROM attained was similar in both cases (HASEL = 77.17°, DC Motor = 85°). However, the force provided by the HASEL actuator was lower than the generated by the motor (HASEL = 0.91 N, DC Motor = 13 N) and below that required to perform daily life activities (Table 4).

Like SMA, SMP can recover a predetermined shape after certain stimuli are applied, such as light, moisture, electricity, and heat[115,116] (**Figure 13**a). Due to their versatility of activation to different stimuli and the possibility of being produced from biodegradable materials, SMPs have been used in different

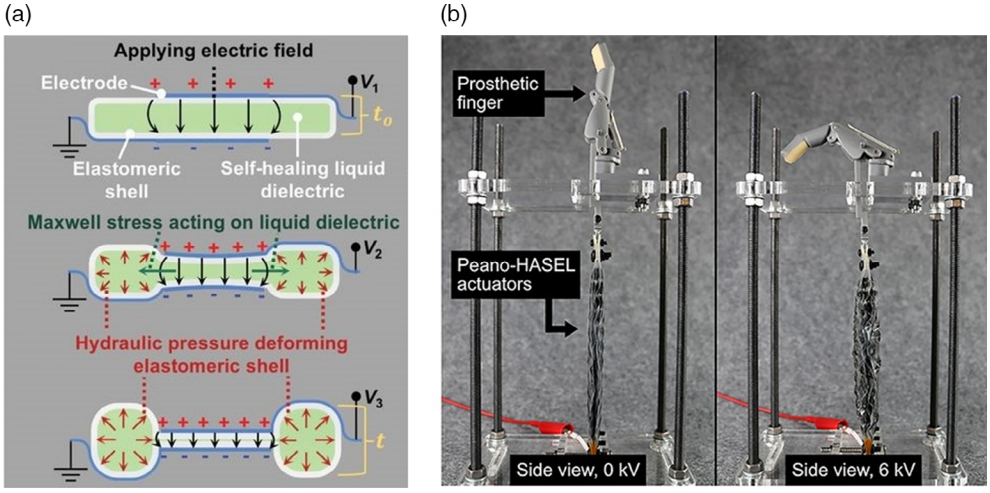

Figure 12. a) HASEL actuator schematic shown at three different applied voltages (where V1 < V2 < V3). Reproduced with permission.[111] Copyright 2018, The American Association for the Advancement of Science. b) An array of Peano-HASEL actuators driving a custom prosthetic finger. Reproduced under the terms of the CC BY license.[114] Copyright 2020, The Authors.

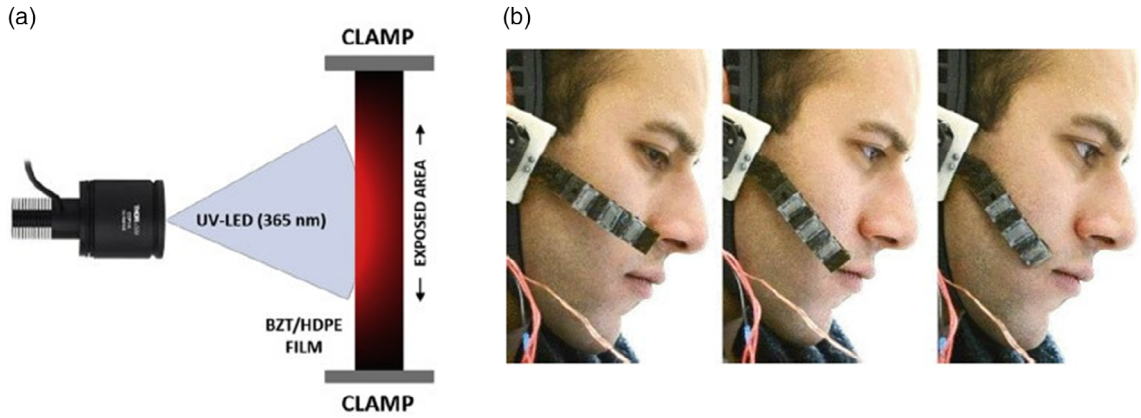

Figure 13. a) Photothermal effect originates from the thermal energy produced by a BZT/HDPE film after exposure to a UV light. Reproduced with permission.[116] Copyright 2020, Elsevier. b) Experiments using a single robot finger for performing the initial reconfiguration utilizing an SMP. Reproduced with permission.[105] Copyright 2017, IEEE.

biomedical applications such as drug delivery, self-tightening sutures, stents, and cellular surgery.[117] However, in the field of rehabilitation robotics, even though they have a high strain, which is a desirable feature (>10%), they are still not used because they present the problem of low stress (1–3 MPa) and slow recovery response (<1 Hz).[33] An example of the incorporation of this technology into the rehabilitation setup is the soft facial rehabilitation robot developed by Firouzeh et al.[105] They incorporate SMPs into a soft robot actuated by a cable-driven system to improve the compliance of the system. The prototype had five points of actuation, and each of them incorporated an SMP to control the stiffness (Figure 13b). The multiple DOFs presented by the robot allowed for initial reconfiguration and activation of different movement patterns depending on the needs of each patient and training. Nevertheless, the switch between different training positions was time consuming (≈10 s) due to the slow transition of the SMP.

3.3. SWRR Based on AMSM Limitations

AMSMs have outstanding flexibility and are lightweight, making them a promising choice to power the next generation of compliant rehabilitation robots. However, the use of these materials is still at the early stage of development, and the devices employing them have fundamental limitations that prevent their successful application.

Most of the robots utilizing AMSM were unable to generate the ROM to perform ADLs. For instance, this problem is related to the limited strain that most AMSM can produce, which is under the skeletal muscle's typical strain (20%). Another requirement that is influenced by the actuator's strain is torque. As the displacement generated by the actuators is linear, and the robots require angular displacements, making the necessary structures to transform linear to angular displacements can lead to a loss of force in the transition. Nevertheless, the main factor in producing the desired torque is the force generated by the AMSM. Concerning the required torque, most of the devices could produce the necessary torque to move the limb against gravity, except for the elbow developed by Behboodi et al.[60] Therefore, most of the evaluated AMSM can generate enough force to be used on wearable robots, except for DEAs that can't deliver high forces with small actuators.

The biggest obstacle for devices based on AMSM seems to be the actuation speed, as most of the reported frequencies and angular velocities were far from the required for ADLs (Table 1–8). However, a possible option would be to use them for rehabilitation therapies where the required speeds to perform the exercises are slower, usually under 100° s^{-1} and frequencies below 0.2 Hz.[118–121] This limitation could also be related to the mathematical models that explain the actuation principles of the AMSM. As the different technologies suffer from different problems like nonlinearity, hysteresis, and electromechanical instability that are difficult to model. The mathematical models are necessary to develop robust control strategies required for high-performance applications.[71,84,122] Hence, most of the evaluated devices used open-loop control schemes toggling between two different predefined levels to alter the length of the AMSM.

Generally, it is possible to categorize the current AMSM for SWRR into two categories: EAPs (DEAs and PVC gels) and thermally activated actuators (SMAs and TCPs). These two groups of actuators translate their limitation into the SWRR. The EAPs present a high actuation speed but low forces (high angular velocity/frequency but low torques). Contrary to the thermally activated actuator that shows low speeds but high forces (low angular velocities/frequency but high torques). Furthermore, the strain seems to be a general limitation (restrict ROM). Nevertheless, these constraints could be lessened with a proper design of the SWRR, as will be explored in the next section.

3.4. Artificial Muscles Enhancements Techniques

Although some SWRRs have initially demonstrated their potential as an assistant rehabilitation tool, all of them have been used in experimental setups in the laboratory environment only. New materials vary in their ability to meet the biomechanical requirements to be useful in the clinical setting. However, SWRRs made of AMSM show great potential for rehabilitation, thanks to their inherent compliance and lightweight. Currently,

an AMSM covering all the essential characteristics to behave like the skeletal muscles does not exist (**Table 9**). However, some of the deficiencies in smart materials can be remedied through the SWRR design.

Table 9. Comparison of artificial muscles Properties.

Device	Actuator technology	Strain [%]	Force [N]	Stress [MPa]	Frequency [Hz]	Size (Length and area or diameter)
Human Body[34]	Skeletal Muscles	20	N/A	0.1	20 Maximum	N/A
Korea Institute of Machinery and Materials[101] (2022)	SMA (spring)	50	0.2	N/A	23.4 s	L: 26 mm D_{SMA}: 0.08 mm D_{Spring}: 0.44 mm
KAIST[100] (2022)	SMA (spring)	N/A	19.28	N/A	N/A	L: N/A D_{SMA}: 0.5 mm D_{Spring}: 2 mm
University of Delaware[60,66] (2020)	DEA	5	10	0.0346	$<$100	L: 39 mm A: 17 $\times$ 17 mm
University of Pisa[68] (2008)	DEA	N/A	0.33	0.000982	N/A	L: 85 mm A: 16 $\times$ 21 mm
Zhejiang University of Technology[61] (2017)	PVC	10	80	0.080	9	L: 200 mm A: 0.001 m^2
Universidad Iberoamericana[82] (2018)	TCP	10	5.4	1.1	$\approx$0.02	L: N/A D: 2.5 mm
Bio-robotics and Smart Systems Laboratory[59] (2017)	TCP	16	3	2	$\approx$0.04	L: 380 mm D: 1.35 mm
MENRVA Group[81] (2016)	TCP	15.	0.9	N/A	0.1	N/A
KAIST[97] (2022)	SMA (spring)	90 mm contraction	11.67	N/A	N/A	L: 120 mm (unstreched) D_{SMA}: 0.5 mm D_{Spring}: 2 mm
Ajou University[92] (2020)	SMA	5	10.5	594	$\approx$1	L: 800 mm D: 0.15 mm
Carlos III University of Madrid[52] (2019)	SMA	4	35.6	181.3	$\approx$0.046 rad s (0.007)	L: 1.5 m Flexion/ Extension L: 2 m Pronation/ Supination D: 0.5 mm
KAIST[98] (2019)	SMA (spring)	33	10	2	0.5 (cooling system with mineral oil)	L: 150 mm D_{SMA}: 0.5 mm D_{Spring}: 2.5 mm
Carlos III University of Madrid[94] (2018)	SMA	5	35.6	181.3	$\approx$0.04	L: 2.2 m Flexion L: 1.7 m Ulnar/Radial deviation D: 0.5 mm
State Key Laboratory of Mechanism System and Vibration[85] (2013)	SMA	10	13.72	280	$>$ 0.1 (Free convection) 5 (Cooling system with water)	L: 220 mm D: 0.25 mm
Wyss Institute[93] (2011)	SMA (spring)	$\approx$66	5	11	$\approx$0.02	L: 175 mm D_{SMA}: 0.25 mm $D_{InnerSpring}$: 0.51 mm
CNR Institute for Energetics and Interphases at Lecco[89] (2009)	SMA	$\approx$3	10	203	$\approx$0.025	L: 2.5 m D: 0.25 mm
Artificial Intelligence Laboratory[88] (2008)	SMA	20 mm contraction	N/A	N/A	N/A	N/A

The required torque depends on two different aspects, the generated force and the lever arm. In the case of force, SMA is the best material to generate forces, unlike DEAs, which struggle to generate high forces. To overcome this limitation, the most used strategy is to employ bundles of actuators that generate the required force.[52,68,81,100] An alternative to increase the torque is to use a larger lever arm. Nevertheless, this strategy presents the drawback that the lever arm length negatively influences the ROM generated by the AMSMs linear displacement.[61,85] The relation of torque and linear displacement with relation to the lever arm could be expressed as

$$\begin{cases} \Delta l = a \sin \Delta\theta \\ T = Fa \end{cases} \tag{18}$$

where Δl is the required linear displacement of the AMSM, a the lever arm, $\Delta\theta$ angular displacement of the joint, T torque, and F is the force.

The linear displacement is related to the strain of the AM. This is another aspect that limits the use of AMSM, as they usually have decreased strain compared to skeletal muscles (<20%). However, thanks to their flexibility and softness, it is possible to place long actuators in small spaces, allowing the device to attain the required displacement without impacting the actuator's performance.[59,89] For SMA, another option to increase the strain is to fabricate springs made of single wires, similar to TCP, when coiled around a mandrel, with the disadvantage of reducing the generated force.[93,123]

In the case of the speed of the motion, it is mainly related to the frequency of the AMSM. DEAs and PVC gel actuators surpassed the frequencies observed in skeletal muscles. In contrast, TCP and SMA actuators experience frequency as the main limitation. The lower frequency of this technology is related to the slow cooling time of the actuators. To improve the speed of the system, actuators with small diameters with lower thermal mass could be utilized as they cool faster.[80,92] Alternatively, one could use external cooling systems,[99,124] but they introduce two issues: increases in weight and power consumption of the device.

In general, to improve the performance of the actuators is necessary to implement closed-loop control strategies that allow the system to provide faster, accurate, and efficient responses.[52,59,78] Applying these closed-loop control strategies usually requires different sensors to read external variables like position and force. Nevertheless, one of the advantages of AMSM is that they present self-sensing properties, allowing for more compact designs as they can be used as sensors and actuators simultaneously.[125–127]

3.5. Summary and Future Developments

The majority of exoskeletons are heavy and bulky, which may cause earlier fatigue or damage to the weak muscles of people with physical disabilities.[9,128] AMSMs have emerged as a solution for this problem thanks to their properties of compliance and lightweight. Nevertheless, they require high voltages and present high-power consumption, making necessary the use of cumbersome equipment such as batteries and high-voltage amplifiers, which are the main contributors to the final weight of the device. Furthermore, power consumption and high voltages are problematic from other perspectives. They can limit the device's use time as well as its autonomy. In some instances, tethering to a power supply may be required,[59] and in the case of the voltages, it may pose a safety risk to the users. However, energy storage and energy transmission are continually being developed, with improvements in the energy density[129,130] and miniaturization of batteries,[131–133] as well as downsized electronic systems,[114] which will ultimately lead to the implementation of SWWR based on AMSM being feasible in the early future.

A specific problem for the thermal base AMSM (SMA and TCP) is the temperatures that they can reach. To generate the maximum force/displacement, they generate temperatures over the pain threshold of humans (44 °C at the dermal/epidermal interface of the skin).[59,134] For this reason, it is still necessary to research design and materials that help to incorporate the artificial muscles seamlessly into the SWRR that can insulate the actuator from the users allowing for comfortable use.[91,135]

AMSM actuators have some properties exceeding those of the skeletal muscles (e.g., SMA generates higher output stress, and DEAs can work at higher frequencies than skeletal muscle). However, currently, there is no AMSM that can integrate all the properties needed to achieve the body's musculoskeletal movement (e.g., AMSM still has a lower strain). Furthermore, there is still a lack of mathematical models that can represent all the physical transformations that the actuators present.[71,84,122] Hence, research on new theoretical models and manufacturing processes that permit or use different compounds to improve the performance of AMSM is still needed.

Based on the data concerning biomechanical requirements related to human movement and the current capability of existing devices (Table 1–8), it is still challenging to use AMSM in SWRR. Nevertheless, using them could be feasible if a proper control strategy is implemented and the assistive task is specific and simple.[59,85] An example is assisting ankle dorsiflexion through the swing phase of gait to help people with "foot drop".[136] This task is in only one plane of motion, does not require fast movement nor high forces given the mass of the foot, and the ROM required is relatively small. Another possibility to start exploring the use of AMSM is to integrate them into hybrid devices with two or more actuation technologies. For instance, it is possible to find devices where the primary actuator generates the forces, and the movements are electric motors, with a smart material to add compliance to the device.[105]

4. Conclusion

It can be concluded that AMSMs are promising actuators to be used in SWRR. However, a better understanding of the minimum biomechanical requirements is necessary to design solutions that can provide a reasonable level of assistance to specific tasks. It seems logical to address relatively simple tasks first before moving toward more complex multifaceted movements that may require high forces and high angular velocities of joint motion with rapid acceleration and decelerations. There is applicability waiting to improve the quality of life of the elderly as well as younger individuals with diseases and

injuries that have left them notably disabled due to muscle weakness.

5. Limitations

The sources analyzed in regard to AMSM are limited to their relationship with SWRR. Therefore, it is not representative of the whole cohort of AMSM currently available for other applications.

In contrast, as this work mainly focuses on the functionality and the gap in the technology of SWRR based on AMSM, artificial muscles for rehabilitation with better performance could exist.

6. Experimental Section

An in-depth literature search was performed, following the search strategy of the Preferred Reporting Items for Systematic Reviews and Meta-Analyses (PRISMA) guidelines.[137] The literature search utilized Scopus and Web of Science databases, using the combination of the following keywords: (Artificial Muscle*) OR (actuat* AND (complian* OR elastic* OR soft)) and (robot* OR wearable OR "active ortho*" OR "active prosthe" OR exoskeleton) and (rehab* OR assistance) not pneumatic*. To make our search as complete as possible, a search through the university library databases was also conducted.

To eliminate areas not linked sufficiently with the aims, articles in the following areas were excluded: a) Non-actuated compliant systems; b) Non-wearable systems; c) Solutions where the soft actuator relies on electric motors or fluidic systems (e.g., pneumatic and hydraulic) as the source of force generation; d) Studies that did not report any mechanical information on the robot; e) Studies not related to either assistance or rehabilitation.

Acknowledgements

This work was partially supported by "Consejo Nacional de Ciencica y Tecnologia" of Mexico (no. 739850).

Conflict of Interest

The authors declare no conflict of interest.

Keywords

artificial muscles, rehabilitation, smart materials, soft robots, wearables

Received: June 8, 2022
Revised: September 6, 2022
Published online:

[1] D. J. Reinkensmeyer, *J. Neuroeng. Rehabil.* **2019**, *16*, 144.
[2] A. Zoss, H. Kazerooni, A. Chu, in *2005 IEEE/RSJ Int. Conf. on Intelligent Robots and Systems*, IEEE, Piscataway, NJ **2005**, pp. 3465–3472.
[3] J. Howard, V. V. Murashov, B. D. Lowe, M. L. Lu, *Am. J. Ind. Med.* **2020**, *63*, 201.
[4] M. Kuroda, S. Nakagawa, H. Mutsuzaki, Y. Mataki, K. Yoshikawa, K. Takahashi, T. Nakayama, N. Iwasaki, *Brain Dev.* **2020**, *42*, 468.
[5] P. Maciejasz, J. Eschweiler, K. Gerlach-Hahn, A. Jansen-Troy, S. Leonhardt, *J. Neuroeng. Rehabil.* **2014**, *11*, 3.
[6] R. Lee, *J. Econ. Perspect.* **2003**, *17*, 167.
[7] Organization, W. H., The global burden of disease: 2004 update, **2008**.
[8] M. Shishehgar, D. Kerr, J. Blake, *Smart Health* **2018**, *7*, 1.
[9] Y. He, D. Eguren, T. P. Luu, J. L. Contreras-Vidal, *Med. Devices Evidence Res.* **2017**, *10*, 89.
[10] Z. F. Lerner, G. M. Gasparri, M. O. Bair, J. L. Lawson, J. Luque, T. A. Harvey, A. T. Lerner, *IEEE Trans. Neural Syst. Rehabil. Eng.* **2018**, *26*, 1985.
[11] R. A. Bos, K. Nizamis, B. F. J. M. Koopman, J. L. Herder, M. Sartori, D. H. Plettenburg, *IEEE Trans. Neural Syst. Rehabil. Eng.* **2020**, *28*, 258.
[12] J. Sancho-Perez, M. Pérez, E. García, D. Sanz-Merodio, A. Plaza, M. Cestari, *Advances in Cooperative Robotics*, World Scientific, Singapore **2017**, pp. 814–822.
[13] T. Bützer, J. Dittli, J. Lieber, H. J. van Hedel, A. Meyer-Heim, O. Lambercy, R. Gassert, 2019 *IEEE 16th Inter. Conf. on Rehabilitation Robotics (ICORR)*, IEEE, Piscataway, NJ **2019**, pp. 108–114.
[14] Z. F. Lerner, T. A. Harvey, J. L. Lawson, *Ann. Biomed. Eng.* **2019**, *47*, 1345.
[15] A. Borboni, M. Mor, R. Faglia, *J. Dyn. Syst. Meas. Contr.* **2016**, *138*.
[16] B. W. Ang, C.-H. Yeow, *IEEE Rob. Autom. Lett.* **2020**, *5*, 3731.
[17] R. S. Araujo, C. R. Silva, S. P. Netto, E. Morya, F. L. Brasil, *Front. Neurosci.* **2021**, *15*.
[18] A. J. Veale, S. Q. Xie, *Med. Eng. Phys.* **2016**, *38*, 317.
[19] D. Rus, M. T. Tolley, *Nature* **2015**, *521*, 467.
[20] Z. Peng, J. Huang, *Appl. Sci.* **2019**, *9*, 3102.
[21] M. Bengisu, M. Ferrara, *Materials that Move: Smart Materials, Intelligent Design*, Springer, Berlin **2018**.
[22] S. Bahl, H. Nagar, I. Singh, S. Sehgal, *Mater. Today: Proc.* **2020**, *28*, 1302.
[23] M. Zhu, S. Biswas, S. I. Dinulescu, N. Kastor, E. W. Hawkes, Y. Visell, *Proc. IEEE* **2022**, *110*, 246.
[24] H. Jin, E. Dong, M. Xu, C. Liu, G. Alici, Y. Jie, *Smart Mater. Struct.* **2016**, *25*, 085026.
[25] U. Gupta, L. Qin, Y. Wang, H. Godaba, J. Zhu, *Smart Mater. Struct.* **2019**, *28*, 103002.
[26] W. Peng, Y. Zhang, J. Gao, Y. Wang, Y. Chen, Y. Zhou, *Sens. Actuators A: Phys.* **2019**, *299*, 111613.
[27] Y. Zhang, L. Huang, H. Song, C. Ni, J. Wu, Q. Zhao, T. Xie, *ACS Appl. Mater. Interfaces* **2019**, *11*, 32408.
[28] C. S. Haines, M. D. Lima, N. Li, G. M. Spinks, J. Foroughi, J. D. W. Madden, S. H. Kim, S. Fang, M. Jung De Andrade, F. Göktepe, Ö. Göktepe, S. M. Mirvakili, S. Naficy, X. Lepró, J. Oh, M. E. Kozlov, S. J. Kim, X. Xu, B. J. Swedlove, G. G. Wallace, R. H. Baughman, *Science* **2014**, *343*, 868.
[29] W.-S. Chu, K.-T. Lee, S.-H. Song, M.-W. Han, J.-Y. Lee, H.-S. Kim, M.-S. Kim, Y.-J. Park, K.-J. Cho, S.-H. Ahn, *Int. J. Precis. Eng. Manuf.* **2012**, *13*, 1281.
[30] R. Granberry, J. Barry, B. Holschuh, J. Abel, *Adv. Mater. Technol.* **2021**, *6*, 2000825.
[31] V. Murphy, B. P. Edmonds, A. L. Trejos, *Actuators* **2021**, *10*, 37.
[32] J. Guo, C. Xiang, T. Helps, M. Taghavi, J. Rossiter, in *2018 IEEE Int. Conf. on Soft Robotics (RoboSoft)*, IEEE, Piscataway, NJ **2018**, pp. 339–343.
[33] J. Zhang, J. Sheng, C. T. O'Neill, C. J. Walsh, R. J. Wood, J.-H. Ryu, J. P. Desai, M. C. Yip, *IEEE Trans. Rob.* **2019**, *35*, 761.
[34] S. M. Mirvakili, I. W. Hunter, *Adv. Mater.* **2018**, *30*, 1704407.
[35] T. Shahid, D. Gouwanda, S. G. Nurzaman, A. A. Gopalai, *Biomimetics* **2018**, *3*, 17.
[36] E. Bardi, M. Gandolla, F. Braghin, F. Resta, A. L. G. Pedrocchi, E. Ambrosini, *J. NeuroEng. Rehabil.* **2022**, *19*.

[37] A. P. Aliseichik, D. A. Gribkov, A. R. Efimov, I. A. Orlov, V. E. Pavlovsky, A. V. Podoprosvetov, I. V. Khaidukova, *J. Comput. Syst. Sci. Int.* **2022**, *61*, 270.
[38] Nematollahi, M., Baghbaderani, K. S., Amerinatanzi, A., Zamanian, H. & Elahinia, M. *Application Of NiTi In Assistive And Rehabilitation Devices: A Review. Bioengineering*, Basel **2019**, p. 6, https://doi.org/10.3390/bioengineering6020037.
[39] T.-Y. Dong, X.-L. Zhang, T. Liu, *Front. Inf. Technol. Electron. Eng.* **2018**, *19*, 1303.
[40] K. L. Mudie, A. C. Boynton, T. Karakolis, M. P. O'Donovan, G. B. Kanagaki, H. P. Crowell, R. K. Begg, M. E. Lafiandra, D. C. Billing, *J. Sci. Med. Sport* **2018**, *21*, 1154.
[41] M. A. Lobo, M. L. Hall, B. Greenspan, P. Rohloff, L. A. Prosser, B. A. Smith, *Phys. Ther.* **2019**, *99*, 647.
[42] A. Kapsalyamov, S. Hussain, P. K. Jamwal, *IEEE Access* **2020**, *8*, 178991.
[43] S. Kawasaki, K. Ohata, T. Yoshida, A. Yokoyama, S. Yamada, *J. NeuroEng. Rehabil.* **2020**, *17*, 1.
[44] K. Nizamis, A. H. A. Stienen, D. G. Kamper, T. Keller, D. H. Plettenburg, E. J. Rouse, D. Farina, B. F. J. M. Koopman, M. Sartori, *IEEE Trans. Med. Rob. Bionics* **2019**, *1*, 88.
[45] M. Cenciarini, A. M. Dollar, in *2011 IEEE Int. Conference on Rehabilitation Robotics*, IEEE, Piscataway, NJ, pp. 1–6.
[46] D. H. Gates, L. S. Walters, J. Cowley, J. M. Wilken, L. Resnik, *Am. J. Occup. Ther.* **2016**, *70*, 7001350010p7001350011.
[47] C. L. Brockett, G. J. Chapman, *Orthop. Trauma* **2016**, *30*, 232.
[48] H. Tanaka, M. Yoshikawa, E. Oyama, Y. Wakita, Y. Matsumoto, *J. Rob.* **2013**, *2013*, 12.
[49] H. S. Nam, H. G. Seo, J.-H. Leigh, Y. J. Kim, S. Kim, M. S. Bang, *Appl. Sci.* **2019**, *9*, 2471.
[50] H. I. Krebs, B. T. Volpe, D. Williams, J. Celestino, S. K. Charles, D. Lynch, N. Hogan, , *IEEE Trans. Neural Syst. Rehabil. Eng.* **2007**, *15*, 327.
[51] J. Rosen, J. C. Perry, N. Manning, S. Burns, B. Hannaford, in *ICAR'05. Proc., 12th Int. Conf. on Advanced Robotics*, Seattle, WA 2005, pp. 532–539.
[52] D. Copaci, F. Martín, L. Moreno, D. Blanco, *IEEE Access* **2019**, *7*, 31473.
[53] K. J. Ganley, C. M. Powers, *Gait Posture* **2005**, *21*, 141.
[54] L.-Q. Zhang, S. G. Chung, S. G. Zhiqiang Bai, S. G. Dali Xu, E. M. T. Van Rey, M. W. Rogers, M. E. Johnson, E. J. Roth, *IEEE Trans. Neural Syst. Rehabil. Eng.* **2002**, *10*, 149.
[55] A. Proto, M. Penhaker, D. Bibbo, D. Vala, S. Conforto, M. Schmid, *Sensors* **2016**, *16*, 524.
[56] C. A. Laubscher, J. T. Sawicki, in *2019 IEEE 16th Int. Conf. on Rehabilitation Robotics (ICORR)*, IEEE, Piscataway, NJ **2019**, pp. 676–681.
[57] R. Vicario, A. Calanca, E. Dimo, N. Murr, M. Meneghetti, R. Ferro, E. Sartori, T. Boaventura, *The 14th PErvasive Technologies Related to Assistive Environments Conf.*, Corfu, Greece **2021**, pp. 359–364.
[58] D. M. Wolpert, *Trends Cognit. Sci.* **1997**, *1*, 209.
[59] L. Saharan, M. J. de Andrade, W. Saleem, R. H. Baughman, Y. Tadesse, *Smart Mater. Struct.* **2017**, *26*, 105048.
[60] A. Behboodi, C. DeSantis, J. Lubsen, S. Lee, in *2020 42nd Annual Int. Conf. of the IEEE Engineering in Medicine & Biology Society (EMBC)*, IEEE, Piscataway, NJ **2020**,pp. 4930–4935.
[61] Y. Li, M. Hashimoto, *Smart Mater. Struct.* **2017**, *26*, 125003.
[62] A. Gonzalez, L. Garcia, J. Kilby, P. McNair, *BioMed. Eng. OnLine* **2021**, *20*.
[63] C. J. Nycz, T. Butzer, O. Lambercy, J. Arata, G. S. Fischer, R. Gassert, *IEEE Rob. Autom. Lett.* **2016**, *1*, 976.
[64] R. C. Browning, J. R. Modica, R. Kram, A. Goswami, *Med. Sci. Sports Exercise* **2007**, *39*, 515.
[65] Y. Bar-Cohen, Y. Bar-Cohen, *Electroactive polymer (EAP) actuators as artificial muscles: Reality, potential, and challenges*, Vol. *136*, SPIE Press, Bellingham, WA **2004**.
[66] A. Behboodi, S. Lee, in *2019 IEEE 16th Int. Conf. on Rehabilitation Robotics (ICORR)*, IEEE, Piscataway, NJ **2019**, pp. 499–505.
[67] B. Shi, X. Chen, Z. Yue, S. Yin, Q. Weng, X. Zhang, J. Wang, W. Wen, *Front. Neurorob.* **2019**, *13*, 63.
[68] F. Carpi, A. Mannini, D. De Rossi, in *Electroactive Polymer Actuators and Devices (EAPAD)*, International Society for Optics and Photonic, **2008**, p. 692705.
[69] Y. Li, M. Hashimoto, *Sens. Actuators A: Phys.* **2015**, *233*, 246.
[70] Y. Li, Y. Maeda, M. Hashimoto, *Int. J. Adv. Rob. Syst.* **2015**, *12*, 175.
[71] Y. Li, M. Guo, Y. Li, *J. Mater. Chem. C* **2019**, *7*, 12991.
[72] M. Yamano, N. Ogawa, M. Hashimoto, M. Takasaki, T. Hirai, in *2008 IEEE Int. Conf. on Robotics and Biomimetics*, IEEE, Piscataway, NJ **2008**, pp. 745–750.
[73] Y. Li, M. Hashimoto, in *2015 IEEE Int. Conf. on Robotics and Automation (ICRA)*, IEEE, Piscataway, NJ **2015**, pp. 2920–2925.
[74] S. M. Mirvakili, A. Rafie Ravandi, I. W. Hunter, C. S. Haines, N. Li, J. Foroughi, S. Naficy, G. M. Spinks, R. H. Baughman, J. D. W. Madden, Simple and strong: twisted silver painted nylon artificial muscle actuated by Joule heating, Vol. 9056, SPIE, **2014**.
[75] S. Y. Yang, K. Kim, J. U. Ko, S. Seo, S. T. Hwang, J. H. Park, H. S. Jung, Y. J. Gong, J. W. Suk, H. Rodrigue, *Soft Rob.* **2022**.
[76] S. A. Horton, P. Dumond, *IEEE/ASME Trans. Mechatron.* **2019**, *24*, 2130.
[77] Y. Almubarak, M. Schmutz, M. Perez, S. Shah, Y. Tadesse, Kraken: A wirelessly controlled octopus-like hybrid robot utilizing stepper motors and fishing line artificial muscle for grasping underwater, **2021**.
[78] M. C. Yip, G. Niemeyer, *IEEE Trans. Rob.* **2017**, *33*, 689.
[79] A. Simeonov, T. Henderson, Z. Lan, G. Sundar, A. Factor, J. Zhang, M. Yip, *IEEE Rob. Autom. Lett.* **2018**, *3*, 1671.
[80] C. S. Haines, G. Niemeyer, in *2018 IEEE/RSJ Int. Conf. on Intelligent Robots and Systems (IROS)*, IEEE, Piscataway, NJ **2018**, pp. 6980–6985.
[81] L. Sutton, H. Moein, A. Rafiee, J. D. Madden, C. Menon, in *2016 6th IEEE Inter. Conf. on Biomedical Robotics and Biomechatronics (BioRob)*, IEEE, Piscataway, NJ **2016**, pp. 1074–1079.
[82] A. G. Patiño, A. Ferrone, C. G. D. Gastélum, C. Menon, in *2018 IEEE 9th Annual Information Technology, Electronics and Mobile Communication Conf. (IEMCON).*, IEEE, Piscataway, NJ **2018**, pp. 620–625.
[83] D. Copaci, E. Cano, L. Moreno, D. Blanco, *Appl. Bionics Biomech.* **2017**, *2017*, 1605101.
[84] Á. Villoslada, N. Escudero, F. Martín, A. Flores, C. Rivera, M. Collado, L. Moreno, *Sens. Actuators A: Phys.* **2015**, *236*, 257.
[85] J. Zhang, Y. Yin, J. Zhu, *Sens. Actuators A: Phys.* **2013**, *201*, 264.
[86] J.-S. Koh, *Materials* **2018**, *11*, 2324.
[87] J. M. Jani, M. Leary, A. Subic, M. A. Gibson, *Mater. Des.* **2014**, *56*, 1078.
[88] D. Jayatilake, A. Gruebler, K. Suzuki, in *2008 4th Int. Conf. on Information and Automation for Sustainability*, Colombo, Sri Lanka **2008**, pp. 395–400.
[89] S. Pittaccio, S. Viscuso, M. Rossini, L. Magoni, S. Pirovano, E. Villa, S. Besseghini, F. Molteni, *J. Mater. Eng. Perform.* **2009**, *18*, 824.
[90] S. Pittaccio, F. Zappasodi, S. Viscuso, F. Mastrolilli, M. Ercolani, F. Passarelli, F. Molteni, S. Besseghini, P. M. Rossini, F. Tecchio, *Hum. Brain Mapp.* **2011**, *32*, 60.
[91] S. H. Koo, Y. B. Lee, C. Kim, G. Kim, G. Lee, J.-S. Koh, *Int. J. Clothing Sci. Technol.* **2020**, *33*, 513.

[92] C. Kim, G. Kim, Y. Lee, G. Lee, S. Han, D. Kang, S. H. Koo, J.-S. Koh, *Smart Mater. Struct.* **2020**, *29*, 055003.
[93] L. Stirling, C.-H. Yu, J. Miller, E. Hawkes, R. Wood, E. Goldfield, R. Nagpal, *J. Mater. Eng. Perform.* **2011**, *20*, 658.
[94] D. Serrano, D. S. Copaci, L. Moreno, D. Blanco, in *2018 IEEE/RSJ Int. Conf. on Intelligent Robots and Systems (IROS)*, IEEE, Piscataway, NJ **2018**, pp. 2318–2323.
[95] D. Copaci, D. Blanco, L. Moreno, in *Proc. of the Joint Workshop on Wearable Robotics and Assistive Devices, Inter. Conf. on Intelligent Robots and Systems (IROS 2016)*, Daejeon, Korea **2016**, pp. 9–14.
[96] A. Villoslada, A. Flores, D. Copaci, D. Blanco, L. Moreno, *Rob. Auton. Syst.* **2015**, *73*, 91.
[97] J. Jeong, K. Hyeon, S.-Y. Jang, C. Chung, S. Hussain, S.-Y. Ahn, S.-K. Bok, K.-U. Kyung, *IEEE Rob. Autom. Lett.* **2022**, *7*, 6028.
[98] J. Jeong, I. B. Yasir, J. Han, C. H. Park, S.-K. Bok, K.-U. Kyung, *Appl. Sci.* **2019**, *9*, 4025.
[99] J. Jeong, K. Hyeon, J. Han, C. H. Park, S.-Y. Ahn, S.-K. Bok, K.-U. Kyung, *IEEE/ASME Trans. Mechatron.* **2021**, *27*, 1046.
[100] K. Hyeon, J. Jeong, C. Chung, M. Cho, S. Hussain, K.-U. Kyung, *IEEE Rob. Autom. Lett.* **2022**, *7*, 10635.
[101] S. J. Park, K. Choi, H. Rodrigue, C. H. Park, *Sci. Rep.* **2022**, *12*.
[102] S. J. Park, C. H. Park, *Sci. Rep.* **2019**, *9*.
[103] A. Behboodi, J. F. Alesi, S. C. Lee, *Soft Robotics In Rehabilitation*, Elsevier, Amsterdam **2021**, pp. 241–258.
[104] A. Washington, J. Neubauer, K. J. Kim, *Soft Robotics In Rehabilitation*, Elsevier, Amsterdam **2021**, pp. 89–110.
[105] A. Firouzeh, J. Paik, in *2017 IEEE/RSJ Int. Conf. on Intelligent Robots and Systems (IROS)*, IEEE, Piscataway, NJ **2017**, pp. 306–313.
[106] T. Mirfakhrai, J. D. W. Madden, R. H. Baughman, *Mater. Today* **2007**, *10*, 30.
[107] W. Mohdisa, A. Hunt, S. H. HosseinNia, *Sensors* **2019**, *19*, 3967.
[108] S. M. Mirvakili, I. W. Hunter, *Adv. Mater.* **2018**, *30*, 1704407.
[109] M. Hao, Y. Wang, Z. Zhu, Q. He, D. Zhu, M. Luo, *Front. Rob. AI* **2019**, *6*, 129.
[110] Q. He, Z. Liu, G. Yin, Y. Yue, M. Yu, H. Li, K. Ji, X. Xu, Z. Dai, M. Chen, *Smart Mater. Struct.* **2020**, *29*, 045013.
[111] E. Acome, S. K. Mitchell, T. G. Morrissey, M. B. Emmett, C. Benjamin, M. King, M. Radakovitz, C. Keplinger, *Science* **2018**, *359*, 61.
[112] S. K. Mitchell, X. Wang, E. Acome, T. Martin, K. Ly, N. Kellaris, V. G. Venkata, C. Keplinger, *Adv. Sci.* **2019**, *6*, 1900178.
[113] N. Kellaris, P. Rothemund, Y. Zeng, S. K. Mitchell, G. M. Smith, K. Jayaram, C. Keplinger, *Adv. Sci.* **2021**, *8*, 2100916.
[114] Z. Yoder, N. Kellaris, C. Chase-Markopoulou, D. Ricken, S. K. Mitchell, M. B. Emmett, R. F. Weir, J. Segil, C. Keplinger, *Front. Rob. AI* **2020**, *7*, 181.
[115] H. Meng, J. Hu, *J. Intell. Mater. Syst. Struct.* **2010**, *21*, 859.
[116] M. R. A. Bhatti, E. Bilotti, H. Zhang, C. W. Bastiaansen, T. Peijs, *Polymer* **2020**, *207*, 122897.
[117] L. Sun, W. M. Huang, Z. Ding, Y. Zhao, C. C. Wang, H. Purnawali, C. Tang, *Mater. Des.* **2012**, *33*, 577.
[118] S.-H. Chen, W.-M. Lien, W.-W. Wang, G.-D. Lee, L.-C. Hsu, K.-W. Lee, S.-Y. Lin, C.-H. Lin, L.-C. Fu, J.-S. Lai, J.-J. Luh, W.-S. Chen, *IEEE Trans. Neural Syst. Rehabil. Eng.* **2016**, *24*, 1199.
[119] Y. N. Wu, M. Hwang, Y. Ren, D. Gaebler-Spira, L. Q. Zhang, *Neurorehabil. Neural Repair* **2011**, *25*, 378.
[120] R. Michnik, et al., *Information Technologies in Biomedicine*, Springer, Berlin **2008**, pp. 551–558.
[121] S. J. Bae, S. H. Jang, J. P. Seo, P. H. Chang, *Front. Hum. Neurosci.* **2017**, *11*.
[122] F. Karami, L. Wu, Y. Tadesse, *IEEE/ASME Trans. Mechatron.* **2020**, *26*, 300.
[123] T. Tsabedze, C. Mullen, R. Coulter, S. Wade, J. Zhang, in *2020 IEEE Int. Conf. on Robotics and Automation (ICRA)*, IEEE, Piscataway, NJ **2020**, pp. 5862–5868.
[124] B. P. Edmonds, A. L. Trejos, in *2019 IEEE 16th Inter. Conf. on Rehabilitation Robotics (ICORR)*, IEEE, Piscataway, NJ **2019**, pp. 368–373.
[125] K. Ly, N. Kellaris, D. McMorris, B. K. Johnson, E. Acome, V. Sundaram, M. Naris, J. S. Humbert, M. E. Rentschler, C. Keplinger, *Soft Rob.* **2020**, *8*, 637.
[126] D. Zhou, W. Zuo, X. Tang, J. Deng, Y. Liu, *Bioinspiration Biomimetics* **2021**, *16*, 045003.
[127] S. Wang, H. Huang, H. Huang, B. Li, K. Huang, *IEEE Rob. Autom. Lett.* **2021**, *6*, 2775.
[128] A. Plaza, M. Hernandez, G. Puyuelo, E. Garces, E. Garcia, *IEEE Rev. Biomed. Eng.* **2021**.
[129] L. Ma, N. Li, C. Long, B. Dong, D. Fang, Z. Liu, Y. Zhao, X. Li, J. Fan, S. Chen, S. Zhang, C. Zhi, *Adv. Funct. Mater.* **2019**, *29*, 1906142.
[130] B. Zhu, X. Wang, P. Yao, J. Li, J. Zhu, *Chem. Sci.* **2019**, *10*, 7132.
[131] M. Synodis, J. Pikul, S. A. B. Allen, M. Allen, in *2019 20th Int. Conf. on Solid-State Sensors, Actuators and Microsystems & Eurosensors XXXIII (TRANSDUCERS & EUROSENSORS XXXIII)*, Berlin, Germany **2019**, pp. 789–792.
[132] B. He, Q. Zhang, L. Li, J. Sun, P. Man, Z. Zhou, Q. Li, J. Guo, L. Xie, C. Li, X. Wang, J. Zhao, T. Zhang, Y. Yao, *J. Mater. Chem. A* **2018**, *6*, 14594.
[133] Q. Liu, G. Zhang, N. Chen, X. Feng, C. Wang, J. Wang, X. Jin, L. Qu, *Adv. Funct. Mater.* **2020**, *30*, 2002086.
[134] J. Lawrence, J. Bull, *Eng. Med.* **1976**, *5*, 61.
[135] J. Berzowska, M. Coelho, in *Ninth IEEE Int. Symp. on Wearable Computers (ISWC'05)*., IEEE, Piscataway, NJ, pp. 82–85.
[136] F. Alnajjar, R. Zaier, S. Khalid, M. Gochoo, *Expert Rev. Med. Dev.* **2020**, *18*, 31.
[137] A. Liberati, D. G. Altman, J. Tetzlaff, C. Mulrow, P. C. Gøtzsche, J. P. A. Ioannidis, M. Clarke, P. J. Devereaux, J. Kleijnen, D. Moher, *J. Clin. Epidemiol.* **2009**, *62*, e1.
[138] Y. Li, M. Hashimoto, in *2016 6th IEEE Inter. Conf. on Biomedical Robotics and Biomechatronics (BioRob)*, IEEE, Piscataway, NJ **2016**, pp. 686–691.
[139] P. Dehail, D. Gagnon, L. Noreau, S. Nadeau, *Spinal Cord* **2008**, *46*, 552.
[140] M. R. Gross, *Anatomical Kinesiology*, Jones & Bartlett Learning, Burlington MA **2020**.
[141] H. Shaaban, C. Pereira, R. Williams, V. Lees, *J. Hand Surg.* **2008**, *33*, 3.
[142] K. A. Mann, F. W. Wernere, A. K. Palmer, *J. Orthopaedic Res.* **1989**, *7*, 304.
[143] A. P. Tjahyono, K. C. Aw, H. Devaraj, W. Surendra, E. Haemmerle, J. Travas-Sejdic, *Ind. Rob. Int. J.* **2013**, *40*, 251.
[144] N. Smaby, M. E. Johanson, B. Baker, D. E. Kenney, W. M. Murray, V. R. Hentz, *J. Rehabil. Res. Dev.* **2004**, *41*, 215.
[145] L. E. Diamond, T. V. Wrigley, K. L. Bennell, R. S. Hinman, J. O'Donnell, P. W. Hodges, *Gait Posture* **2016**, *43*, 198.
[146] N. B. Reese, W. D. Bandy, *Joint Range of Motion and Muscle Length Testing-E-Book*, Elsevier Health Sciences **2016**.
[147] T. B. Palmer, N. D. Jenkins, J. T. Cramer, *J. Sports Sci.* **2013**, *31*, 867.
[148] B. F. Mentiplay, M. Banky, R. A. Clark, M. B. Kahn, G. Williams, *Gait Posture* **2018**, *65*, 190.
[149] S. R. Freitas, J. R. Vaz, P. M. Bruno, M. J. Valamatos, P. Mil-Homens, *Physiol. Meas.* **2013**, *34*, 1483.
[150] S. Pittaccio, S. Viscuso, E. Beretta, A. C. Turconi, S. Strazzer, *Prosthet. Orthot. Int.* **2010**, *34*, 305.
[151] J. G. Neely, R. G. Pomerantz, *Laryngoscope* **2002**, *112*, 1562.

Alberto Gonzalez-Vazquez received a B.S. degree in electronic engineering from Instituto Tecnologico de Morelia and an M.S. degree in biomedical engineering from Politecnico di Milano. He is currently a Ph.D. student at Auckland University of Technology, New Zealand. His research interests include wearables, artificial muscles, and soft robots applied to rehabilitation.

Lorenzo Garcia. BioDesign engineer and academic within the Mechanical Engineering Department at Auckland University of Technology (AUT), New Zealand, holds a B.S. in applied physics, a B.E. in mechanical engineering, and a Ph.D. in biomedical engineering. He is the theme leader in Biomechanics and Biomechatronics Design within the BioDesign Lab Institute. He develops three research lines: Rehabilitation and assistive technologies; tools for trauma and orthopedic medicine, and bio-inspired devices for health care and conservation of nature.

Jeff Kilby. I am presently a senior lecturer in electrical and electronic engineering at Auckland University of Technology (AUT), Auckland, New Zealand. My postgraduate qualifications include a Ph.D. titled "Development of a New Multi-channel Electrode and Signal Processing for Surface Electromyography Signals Feature Extraction" and an M.Eng. (Hons) titled "Wavelet Analysis and Classification of Surface Electromyography Signals", both awarded by AUT. My primary research activity is in biomedical instrumentation and feedback, signal processing, and wireless sensor technology related to surface electromyography. An active member in the following research institutes: Biodesign Lab and Health and Rehabilitation Research Centre at AUT.